

MÁSTER INTERUNIVERSITARIO EN ASTROFÍSICA UCM-UAM

MASTER THESIS

**Absolute photometry and Night Sky
Brightness with all-sky cameras**

Author:

Miguel NIEVAS

Supervisors:

Prof. Jaime ZAMORANO

Prof. José Luis CONTRERAS

*A thesis submitted in fulfilment of the requirements
for the degree of Master in Astrophysics*

Departamento de Astrofísica y Ciencias de la Atmósfera
Departamento de Física Atómica, Molecular y Nuclear

June 2013

Course credits: 24

UNIVERSIDAD COMPLUTENSE DE MADRID
UNIVERSIDAD AUTÓNOMA DE MADRID

Abstract

Facultad de Ciencias Físicas
Departamento de Astrofísica y Ciencias de la Atmósfera
Departamento de Física Atómica, Molecular y Nuclear

Master in Astrophysics

Absolute photometry and Night Sky Brightness with all-sky cameras

All-sky cameras have proven to be powerful tools to continuously monitoring the sky in a wide range of fields in both Astrophysics and Meteorology.

In this work, we have developed a complete software pipeline to analyze the night CCD images obtained with one of such systems. This let us to study typical parameters used in Astrophysics to characterize the night sky quality, such as the Sky Brightness, the Cloud Coverage and the Atmospheric Extinction, how they evolve over the time and their variability.

Using our software, we analyzed a large set of data from AstMon-OT all-sky camera at Teide Observatory. Results from this work have been applied in the support to the spanish CTA site proposal at Izaña, Tenerife and are being discussed within the CTA consortium.

A comparison with data from other devices that have been used in site characterization such as the IAC80 telescope is also presented. This comparison is used to validate the results of the analysis of all-sky images.

Finally, we test our software with AstMon-UCM and DSLR cameras. Some general recommendations for the use of DSLR cameras are provided.

Acknowledgements

I must thank Jose Luis Contreras and Jaime Zamorano, the directors of the present work, the possibility to collaborate in their respective research groups. This has been fundamental to build the main ideas necessary to write this master thesis.

They have been very involved in the development of the software, giving constant feedback of issues that needed to be improved. I must also thank Jose Luis and Jaime their help on the interaction with the rest of the CTA community.

‘Oficina técnica de protección de la calidad el cielo’, the Sky Quality Group (particularly Casiana Muñoz) and Support Astronomers Group (Rafael Barrena among others) of IAC are worth of mention for giving me access to the AstMon-OT raw data and for giving the opportunity to work in this field in the IAC summer scholarship 2012. The IAC80 data obtained during this summer was fundamental to validate the results of AstMon-OT data and PyASB software.

I thank also the feedback from the spanish CTA site working package, especially Irene Puerto and Markus Gaug, for giving ideas on the cloud coverage detection and night sky background measures with AstMon-OT. The comparison with Atmoscope photometer data and other sources of cloud coverage detection gave me an important sanity check for the analysis of AstMon data.

I give a credit also to Alejandro Sánchez and Francisco Ocaña. They provided useful DSLR test images at the Roque de los Muchachos Observatory and Yebes Astronomical Center for training the PyASB image analysis algorithms and also fireball detection notices that were compared to AstMon-UCM and let us to set limits to the sensibility of AstMon camera to such events.

Contents

Abstract	ii
Acknowledgements	iii
List of Figures	v
List of Tables	vii
1 Introduction	1
1.1 Motivation. Night Sky Quality	1
1.2 All-sky cameras in Night Sky Quality studies	2
2 AstMon all-sky camera	3
2.1 Device description	3
2.1.1 Component list	3
2.2 Control software	4
2.2.1 Initial calibration	4
2.2.2 Available data	5
3 PyASB: All-Sky Brightness pipeline	6
3.1 AstMon software analysis	6
3.2 PyASB image analysis software	6
3.2.1 Data Input	7
3.2.2 Processing	8
3.2.2.1 Image Analysis	8
Image calibration	10
Dark signal subtraction	10
Star detection	10
3.2.3 Data Output	14
3.3 Long-term data analysis	14
4 Results	16
4.1 Izaña site characterization	16
4.2 Night Sky Background	16
4.3 Extinction	17
4.4 Cloud coverage	22
4.5 Comparison of AstMon data with IAC80	24
4.6 Moon effect on the night sky background	25
4.7 The Milky Way effect on the night sky background	27
4.8 Other effects	28
5 Conclusions	30
A AstMon-UCM	i
A.1 Madrid. A light polluted sky	i
A.2 Night Sky Background	i
B Digital Cameras on site testing	iv
B.1 Description	iv
B.2 Testing PyASB with digital cameras	v
B.3 Results	vi
Bibliography	ix

List of Figures

2.1	AstMon UCM as installed in the roof of the physics building at Universidad Complutense de Madrid, Ciudad Universitaria.	3
2.2	AstMon control software, which acquires the science and calibration images.	5
3.1	Organogram showing the complete PyASB all-sky image analysis workflow, showing the three main blocks: The FTP module that retrieves the images from the server, the PyASB image analysis and the Summary (reduced data) long-term analysis.	9
3.2	Histogram of values measured in the corners of V band images for AstMon-OT from February 2012 to May 2013.	10
3.3	Comparison between a hazy (left) and clear (right) night in the star detection process. Note that only the Moon, Jupiter and the brightest stars can be seen in bad conditions. In contrast, we can detect more than 100 stars in a single frame if the night is clear.	11
3.4	Example of Bouguer extinction law fit done with PyASB.	12
3.5	B-band sky background map at Izaña's observatory. The Milky Way is crossing the zenith.	13
3.6	Comparison between cloudy (left) and clear (right) nights in the cloud detection process. It is clear that an all-sky camera equipped with a fisheye lens can serve as a robust cloud detector, very useful for remote observations with robotic telescopes. However, fine tune-up for each system is needed to correctly estimate the cloud coverage with star detection percentage.	13
4.1	Artist impression of the Cherenkov Telescope Array at Izaña.	16
4.2	Zenithal Night Sky Brightness histogram measured with AstMon-OT.	18
4.3	Zenithal night sky background evolution over the time from AstMon-OT. Only clear nights are shown. The median and the interval that contains the 90% of the data is given. To improve readability, only some error bars are plotted.	19
4.4	Upper graph: Seasonal changes on the night sky background in Johnson V at Izaña. Lower graph: 'Average' night sky background evolution over the night. In both graphs the boxes represent the 1/4 quartile, the median (red line) and the 3/4 quartile. The error bars represents the limits of the data (not counting outliers).	20
4.5	Measured extinction values found at Izaña. Only cloudless images are shown.	21
4.6	Saharan dust as seen from satellite images.	22
4.7	Johnson V extinction values found at Izaña, averaged within seasons. As with the NSB nighttime evolution, the boxes limits and red lines represent the quartiles and the median, whereas the errorbars shows the data limits (excluding outliers).	22
4.8	Left: Extinction slope-slope diagram for AstMon-OT. July 2012 data (a exceptional case with nearly no aerosol-free days) is marked in orange. Right: Color-color diagram for AstMon-OT. July 2012 data is also marked in orange.	23
4.9	Cloud coverage histogram at Teide Observatory.	24
4.10	Moon position and phase effect in the zenithal night sky background. The first two graphs refers to Johnson B and V measures. The bottom is a composed B-V map.	26
4.11	Milky Way effect in different photometric bands.	28
4.12	Airglow as seen from the ISS spacecraft.	28
A.1	Zenithal Night Sky Background evolution over the time from AstMon-UCM in V band. The median and the interval that contains the 90% of the data is given. Error bars are shown for some selected points as reference.	ii
A.2	Night sky background evolution over the night at UCM Observatory.	ii
A.3	Zenithal Night Sky Background histogram at UCM Observatory.	iii
B.1	Left: Digital camera sensor unit. IR-cut filter is visible (cyan color with purple reflection). Right: Scheme of a Bayer matrix with RGGB layout in a sensor.	v
B.2	Left: Set-up of a DSLR camera to obtain all-sky images. Right: Crop of Villaverde's night sky image with Canon EOS 5D II and Sigma 8mm fisheye.	v

- B.3 **Left:** Vignetting table with the angle (from the optical axis) and the relative illumination. Values from $\text{Angle} > 90^\circ$ are invented, and their only purpose is to populate the non-illuminated parts of the image with valid float values. The real data ($< 90^\circ$) has been obtained from [1]. **Right:** Generated flat field for the Canon 5D camera with our software. vi
- B.4 **Upper:** Star detection process in Canon 5D Mark II + Sigma 8mm at Villaverde del Ducado (left) and Yebes astronomical center (right), both in Guadalajara but at different distances (100km and 50km) from Madrid. **Lower:** After calibrating the system with star fluxes, night sky background map is computed. Note the glow at West, caused by Madrid and Corredor del Henares light pollution. The glow is more prominent in Yebes (it is closer to Madrid). vii
- B.5 Photometric fit of the data from two observations with the DSLR camera using similar parameters. The green linear fit is done for the filtered data (purple points) after removing variable stars (red points), low signal stars or those with less precision than 0.1^{mag} (crosses shaped points) and stars with more than 0.3^{mag} of differences between images. **Left:** Yebes astronomical center (Guadalajara, $\sim 50\text{km}$ from Madrid) data. **Right:** Villaverde del Ducado (Guadalajara, $\sim 130\text{km}$ from Madrid) data. viii

List of Tables

2.1	Main characteristics of the CCD	4
4.1	Comparison of AstMon-OT data with Kidger measured values of extinction at Canary Islands' International Observatories (uncertainties are derived using the decile values from Table II on Kidger 2006). In AstMon, we use also the deciles.	17
4.2	Effective (mean) λ s used in extinction slope-slope diagrams [2]. A better estimation of this effective extinction weighted- λ for each AstMon band should be considered in the future, but for our purposes this simple mean estimation is enough.	20
4.3	Median of Night Sky Background taken with IAC80-OT in the sky quality routine observations of the IAC. Comparison with values for Roque de los Muchachos taken at Isaac Newton Group is shown (http://www.ing.iac.es/Astronomy/observing/conditions/skybr/skybr.html).	24
4.4	Comparison of our AstMon-OT measures with IAC80 Night Sky Background data.	25
4.5	Parameters of the Milky Way effect model on the night sky background.	28
A.1	Comparison of measured night sky background between OT and UCM sites.	i

Chapter 1

Introduction

1.1 Motivation. Night Sky Quality

Night sky quality is an important factor that set limits on where a new observatory can be built. It is not only needed that the site has a dark sky, but also that the conditions are stable in the long term.

It is a requisite that the site has a high percentage of clear and usable nights. For optical observations a high number of photometric nights per year is needed. In this sense, several attempts have been made around the world to study the astrophysics conditions of some candidates proposed to house new observatories.

For already existing observatories, these measures are important to show the institutions how to fight the night sky degradation with the increasing human activities near the observatories. Here we have the example of the Palomar observatory, which was initially built to observe faint objects in the sky. Since 1934, its effectiveness in some fields has been gradually decreasing due to the uncontrolled urbanization in the South California[3].

In Spain, we have also an excellent example at Canary Island with mixed readings. Canary Island institutions have some night sky protection programs in place[4–6]. In the case of Tenerife, they helped to slow down the increasing effect of the light pollution at Izaña's Observatory but until now they have not reduced the night sky background already present at the observatory. The degree of protection seems to be stronger in La Palma, with a night sky background similar of those we can find in first line skies such as Namibian, Chilean or Hawaii sites.

Night sky quality measures have also some applications in non-astrophysics fields. In biology and medicine, it is interesting to see how the night light pollution can affect the circadian rhythm in animals of different ecosystems and even in our own health[7]. Some studies have raised the alarm about the effect of circadian cycles in the proliferation of some types of cancer[8]. Light pollution is also a great problem for nocturnal animals, that depend on the darkness of the sky to hunt, navigate and reproduce[9, 10]. Nowadays, the link between the light pollution and this health and ecological issues is being addressed by some research groups, but with a lot of uncertainties.

Last but not least is the fact that, in light polluted sites, night sky background measures are also useful to optimize energy saving policies. It is worth of mention that there are important research groups in cities like Hong Kong, Berlin and Madrid that are currently working on this field.

1.2 All-sky cameras in Night Sky Quality studies

All-sky cameras provide a excellent tool for studying the night sky quality. They give both the spatial and time resolution (all the positions in the sky are covered at the same time) needed to monitor parameters that are variable within minutes or hours, such as the cloud coverage, and to study other indicators such as the night sky background that will change depending on the position in the sky.

They are also dedicated instruments, so there is no need to use telescope observation time, which could then be used for other purposes.

In addition, with the adequate software, they can be operated autonomously and results can be used immediately to make real-time decisions that may optimize the astrophysical observations on an observatory.

Long-term analysis can also bring useful statistics about parameters such as the number of observable nights or the number of photometric nights, which are often used as indicators of the quality of a given observatory.

These advantages are often accompanied with several problems that need to be solved. The first one is the instrument calibration, because all-sky images tend to suffer from severe distortion, vignetting and other optical/electronic defects. The second is the software creation, as we want robust algorithms that do not rely on user interaction and data filtering.

The main goal of this work is, thus, to analyze and try to give solutions for both problems. In chapter 2 we present the AstMon all-sky camera characteristics and the data set. In chapter 3, PyASB image analysis software is described. Chapter 4 summarizes the main results obtained in long-term analysis of the AstMon-OT data. Finally, two appendices are dedicated to other devices: AstMon-UCM (a similar device to the AstMon-OT, but placed in a light polluted environment) and DSLR cameras, portable, easy to use and cheap devices that can be used in sky quality analysis.

Chapter 2

AstMon all-sky camera

The ‘All-Sky Transmission MONitor’, AstMon hereafter, is an all-sky camera designed by Jesús Aceituno at the company iTec Astronomica S.L. Several units of this device have been produced and installed at:

- CAHA (Calar Alto) observatory, near the $3.5m$ telescope (Almería).
- Doñana national park (Huelva).
- Roof of the physics building at Universidad Complutense de Madrid (Madrid) [AstMon-UCM].
- Teide Observatory (Tenerife) [AstMon-OT].
- Javalambre Observatory (Teruel).

In this work, we have been working with two of them, AstMon-OT (Tenerife) and AstMon-UCM (Madrid)[[2.1](#)], but there are plans to collaborate with the analysis on the Doñana’s unit in the future.

2.1 Device description

AstMon is a scientific device whose main goal is to continuously monitor the astronomical conditions at a given place. As a product of its observations, all-sky images at different bands, extinction measures, cloud coverage and sky brightness maps are generated.

2.1.1 Component list

AstMon is a complete device that consists in:



FIGURE 2.1: AstMon UCM as installed in the roof of the physics building at Universidad Complutense de Madrid, Ciudad Universitaria.

Pixel pitch	$5.4 \times 5.4 \mu m$
Gain	$0.5e^-$ (selected in AstMon) and $1.1e^-$ (available)
Dynamic range	16 bits
Read noise	typically $8e^-$
Dark current	$1e^-/px/s$ at $0^\circ C$
Read time	typically 21s, depends on computer.
Connectivity	USB 2.0

TABLE 2.1: Main characteristics of the CCD

- **CCD camera:** QSI 583 WS, equipped with a Kodak 8300 monochrome sensor, with active peltier cooling and a filter-wheel with interchangeable filters. Temperature is fixed at $-15^\circ C$ during image acquisition with a peltier+fan unit with a thermostat. This is done mostly to reduce the thermal dark current and stabilize it along the night, see Table 2.1.
- **filter set:** AstMon-UCM has a set of standard Johnson-Cousins B,V and R filters. AstMon-OT also incorporates a Johnson U filter, although the quantum efficiency of the camera at those wavelengths is rather poor.
- **fisheye lens:** Sigma 4.5mm F2.8 EX DC HSM Circular Fisheye. This fisheye lens produces a standard Zenithal Equal Area projection¹.

As the CCD camera and objective lens are somewhat delicate, AstMon is placed in a waterproof case with a clear methacrylate dome on top of it. This dome needs to be cleaned every month to avoid loosing the exceptional transmission properties of the methacrylate in visible bands.

2.2 Control software

In order to make useful measures with the device described above, *iTec Astronomica* developed a complete software to perform the image acquisition, calibration and the process of generating extinction, cloud coverage and sky brightness measures.

The main problem with this software is that one cannot develop it further as it is proprietary (closed source model) and we will not be able to fix its glitches in the future without the help of its author.

In AstMon-UCM for example, the software has not been able to make a zero-point calibration since it has been installed in fall 2010. Although the zero-point should be stable from night to night, we can expect some long-term changes if dust is deposited on the surface of the dome.

2.2.1 Initial calibration

The initial photometric calibration of AstMon-UCM was performed on November 2009. On July 2010 AstMon-UCM was set up in the UCM urban observatory and the instrument was calibrated also astrometrically. AstMon-OT was installed at the end of 2011.

¹ZEA projection has the property of giving the same pixel sky projected area for every pixel. See [11] for further details

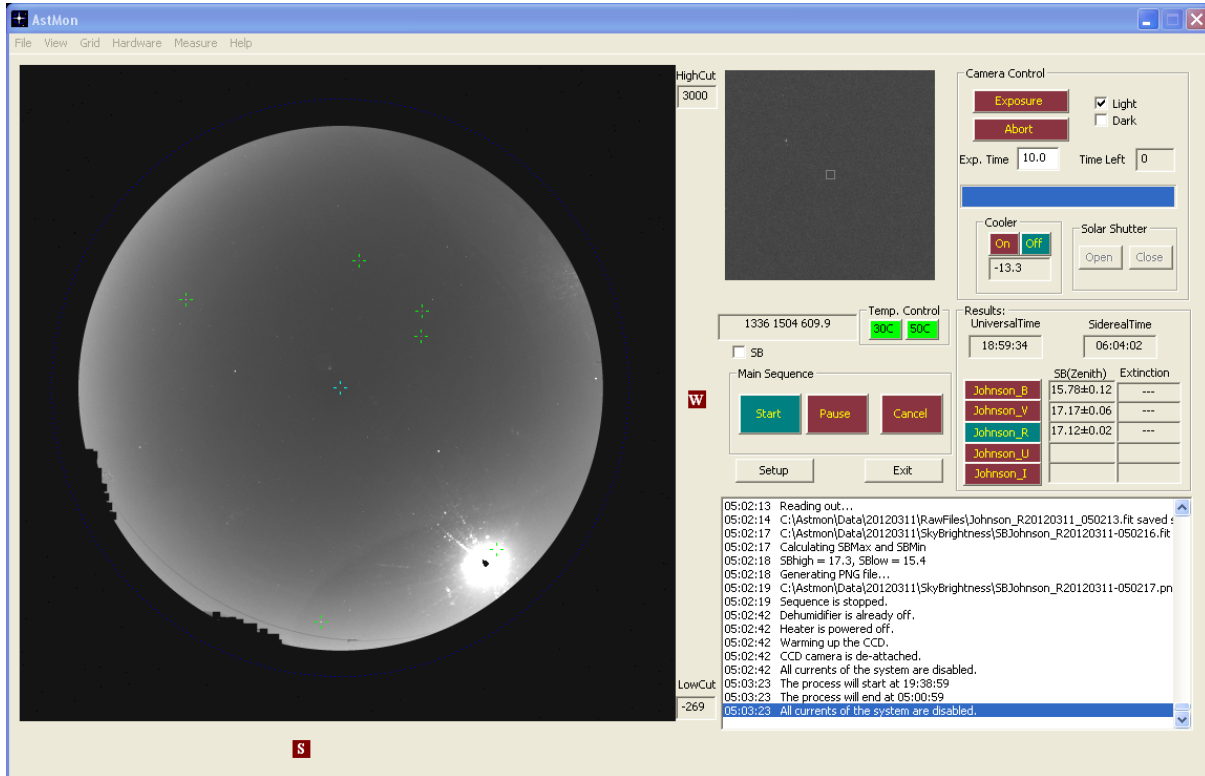


FIGURE 2.2: AstMon control software, which acquires the science and calibration images.

2.2.2 Available data

AstMon-UCM has been taking scientific data since July 2010 until now with some minor gaps due to computer freezes and crashes and a problem we had with the solar shutter in winter 2010/2011. In total, we have collected $\gtrsim 100000$ images (115000 as of May 17, 2013) in three photometric filters (Johnson B,V,R) with AstMon-UCM, our main camera.

With AstMon-OT (the one we're using at the CTA site testing), we have images from January 2012 until now available in a FTP repository. In total, we have ~ 25000 images in U, B, V and R photometric bands, although we discarded the ones in U band due to the extremely poor signal and the difficulties to fit the stars shapes (very elongated and defocused due to poor focus, large exposures needed to get an acceptable signal and low brightness of many of the catalog stars) to perform the calibration.

Chapter 3

PyASB: All-Sky Brightness pipeline

3.1 AstMon software analysis

In [12] the first results obtained with AstMon-UCM and its control and analysis program were presented. In this work the researchers realized that the program that operates AstMon, although fully automatic, has some problems that cannot be solved easily.

First of all, it is closed-source, so one cannot develop it further with new features, fixes and corrections. This is a problem for scientific purposes, but it could be acceptable as long as the main purpose of the instrument is to control the sky conditions in an observatory but not to make a scientific use of the data.

The second problem, arising also from how the software has been written, is related to repeatability. When doing an scientific experiment, we need to describe it carefully in order to let others to replicate and check the results if they want. With AstMon however, the intermediate results are not provided to the user. Only the raw image (without the calibration files) and the final results are saved into files (extinction measures for each star, night sky background and cloud coverage map). AstMon software in that sense is like a *black box*. We can work with the results it produces: cloud maps, sky brightness maps and extinction data, but we cannot reproduce them easily, nor tune-up/fix the method. The procedure is fixed with some default internal methods and routines and is also fixed for the hardware AstMon uses (it cannot be extended for other systems).

Because of that, we decided after [12] that our next steps would be to write an independent and open source software to analyze all the raw data in a similar way. The software should also be scalable to other systems.

3.2 PyASB image analysis software

The first functional version of the new analysis software was written during the [13] coursework. By the end of the spring 2012, we tested it successfully with images taken both with AstMon-UCM and some digital cameras equipped with fisheye lenses.

However, we decided to rewrite the software for this work almost completely to make it more scalable and to improve the image analysis pipeline. This took several months of work, until the 2nd release of the analysis software (hereafter PyASB, from Python All-Sky Brightness) became ready.

Nowadays, the PyASB software accounts more than 9000 lines of python code, including the image analysis module (~ 3000 lines of code), the long-term analysis utility (~ 4200 lines of code) and the auxiliary modules:

- A synthetic flatfield generator. An utility to build flatfields from two component flats (low and high frequency or a radial response plus a high frequency flat) or a single one (radial response / relative illumination of the system).
- RAW (Canon CR2 and Nikon NEF formats) to FITS converter, including debayering.
- Solar dynamics utility. Fetches data from the SDO repository to analyze the influence of the solar activity in our measures.
- FTP utility. Retrieves All-Sky images from a FTP server.

The code has been released under the GPL version 3 license, which grants users to read, share, modify and adapt the software to match their own requisites. Commercial use, modification and/or redistribution is also allowed as long as the original code and the modifications are provided with the same terms of use and license.

The software will be publicly available when it reaches a mature state of development. However, we supply the latest release with the electronic version of this paper.

3.2.1 Data Input

In order to perform the full analysis, PyASB needs some previously-known information as input. The user must set up a configuration file that includes:

- Geographic data about the observatory (or the place where the camera is set-up)
- The astrometric calibration of the images (here we must include, assuming a Zenithal Equal Area projection, the radial scaling factor R_θ of the image, the azimuth zero point ϕ_0 in degrees, and the X-Y offset in pixels (x_0 and y_0) of the zenith from the center of the image), giving:

$$x = -R_\theta \sin(\phi - \phi_0) + x_0 \quad y = R_\theta \cos(\phi - \phi_0) + y_0 \quad (3.1)$$

$$R_\theta = \frac{180^\circ}{\pi} \sqrt{2(1 - \sin(\theta))} = \frac{360^\circ}{\pi} \sin\left(\frac{90 - \theta}{2}\right) \quad (3.2)$$

Note that this is a first approach to the general problem of determining the positions in the image, valid only if the pointing error of the instrument axis to zenith is only few degrees at most.

If we need a general solution for random pointings, we would need another 2 parameters, whose effect is to change the ‘effective geographical location’ of the camera¹. This has been implemented in the software and successfully tested, but requires a little more work by the user to calibrate the extra parameters.

¹A change in the optical axis pointing direction is the same as pointing at the zenith in a different place in the Earth.

- Photometric catalog that contains a list of stars with their astrometry (*RA* and *DEC* coordinates) and photometric properties. We have selected, like the original AstMon program, the *Ducati 2002* catalog, which contains the astrometric and photometric properties of stars up to $V \sim 16$ in 11 different photometric bands.
- CCD image bit depth. Needed to determine if the star is saturated.
- Image analysis parameters:
 - Star detection altitude threshold.
 - Aperture photometry base radius.
 - Detection threshold for the star flux (in sigmas, background as reference).
 - Threshold (sigmas) for point removal in the Fit².
 - Maximum magnitude of stars to be loaded from the catalog (the catalog is sorted by magnitudes).
 - Maximum number of stars to be loaded from the catalog (reduces the load time).

As of the image, PyASB takes an all-sky fits file with data for a single filter. The default behavior is to assume a Zenithal Equal Area projection, but other projections may be implemented easily in the future.

3.2.2 Processing

The complete PyASB software can be separated in several individual parts. We will describe them below. They are also summarized in the diagram of Figure 3.1.

3.2.2.1 Image Analysis

This set of modules and scripts should be considered the main part in the analysis software and is managed through the PyASB launcher script.

To start the launcher script, the user must provide as input options both the image and the configuration file, as relative or full paths. The user must also decide which tables and plots should be generated by PyASB software. This is done by giving some ‘-oX’ parameters with an optional path (in case we are not interested in seen the results on screen but we want them dumped into files).

Example of use:

```
python pyasb_launcher.py -c myconfigfile.cfg -i ~/myimage.fit \
-om ~/starmap.png -ob -os ~/skybrightnessmap.png \
-oct ~/cloudcovertable.txt
```

²We use a robust Theil-Sen regression fit estimator with a Kendall-Tau correlation coefficient for the sigma clipping of the data. See [13] for further details.

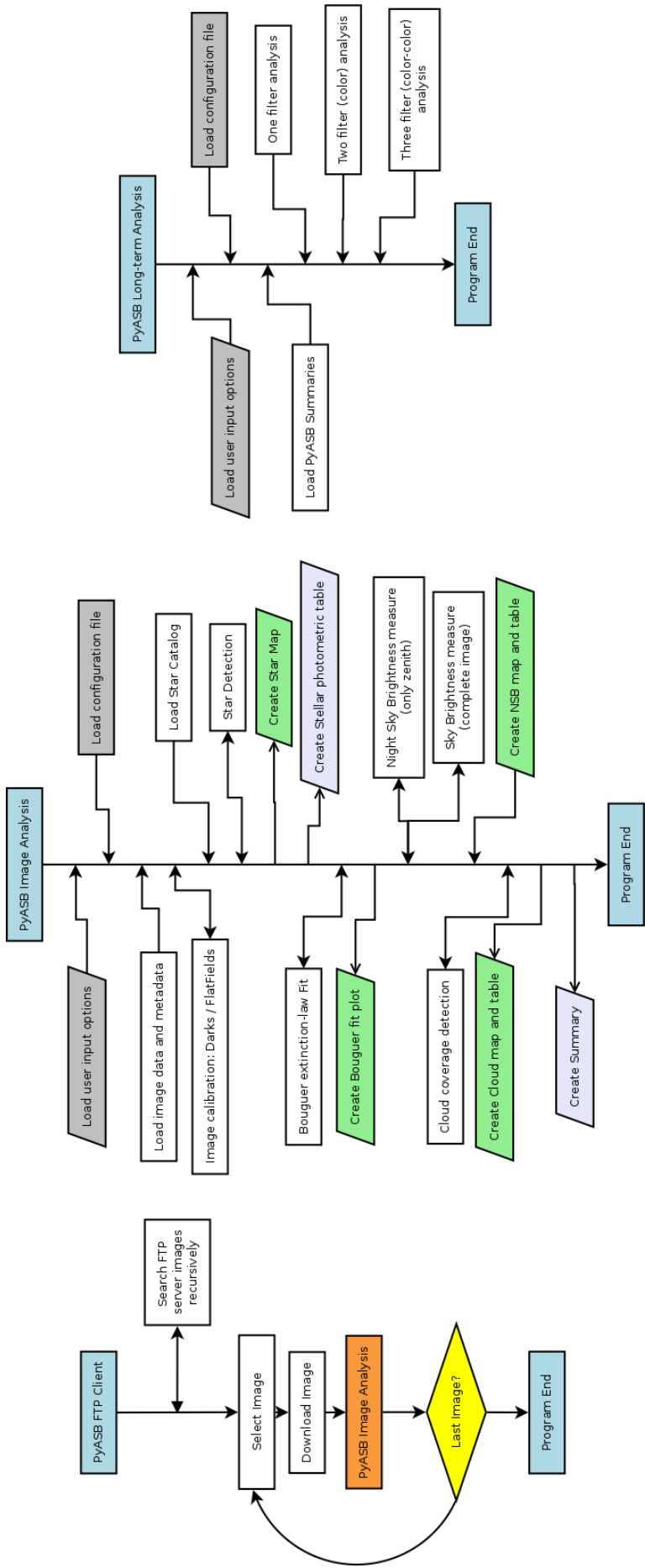


FIGURE 3.1: Organogram showing the complete PyASB all-sky image analysis workflow, showing the three main blocks: The FTP module that retrieves the images from the server, the PyASB image analysis and the Summary (reduced data) long-term analysis.

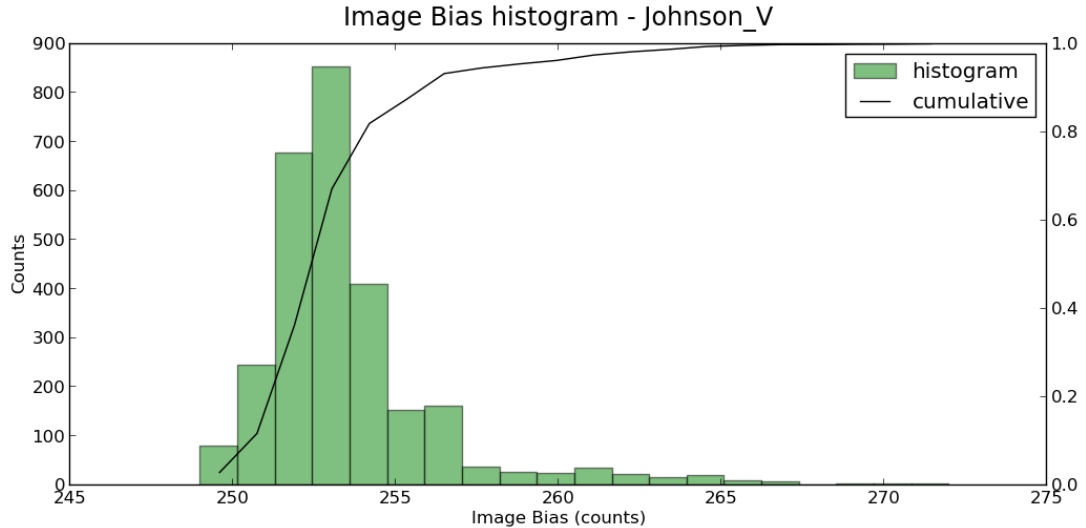


FIGURE 3.2: Histogram of values measured in the corners of V band images for AstMon-OT from February 2012 to May 2013.

This will show on screen the Bouguer calibration fit ('-ob') and will save into files the star map, the night sky background map and the cloud coverage table.

The program's manual page includes the description of all valid input options. It can be accessed by using '-h' as input option.

Image calibration After setting the user options and pressing Enter, the software begins the analysis sequence. First of all, the image is loaded in memory and the data is calibrated with Darks and FlatFields if possible in order to remove the dark signal and flatter the pixel response.

$$SCI(i,j) = \frac{IMG(i,j) - DARK(i,j)}{FF(i,j)} \quad (3.3)$$

Dark signal subtraction We have found that dark current changes in AstMon between images³. This could be caused mainly by changes in the temperature of the CCD, but also by electronic noise due to the power supply of the device. We found that the best way to subtract this intrinsic noise is to use the non-illuminated corners of the science image. This correction, although small, has to be taken into account due to the small background flux that typically exists in dark sites like Izaña's.

The implementation of this modification implies the change $DARK(i,j) \rightarrow DARK(i,j) + CornerBias$ in (3.3), where $CornerBias$ is the median of the pixel values in the non-illuminated corners of the image.

Star detection When the data is reduced, the program looks for stars in the field based on a previously found astrometric solution and data from a star catalog. It should be noted that AstMon is designed to be in a fixed position.

³Statistical analysis shows variations within $\sim 5 - 10$ counts for 40s exposure images, see Figure 3.2. In B band, this variations are of the same order of magnitude of the background signal.

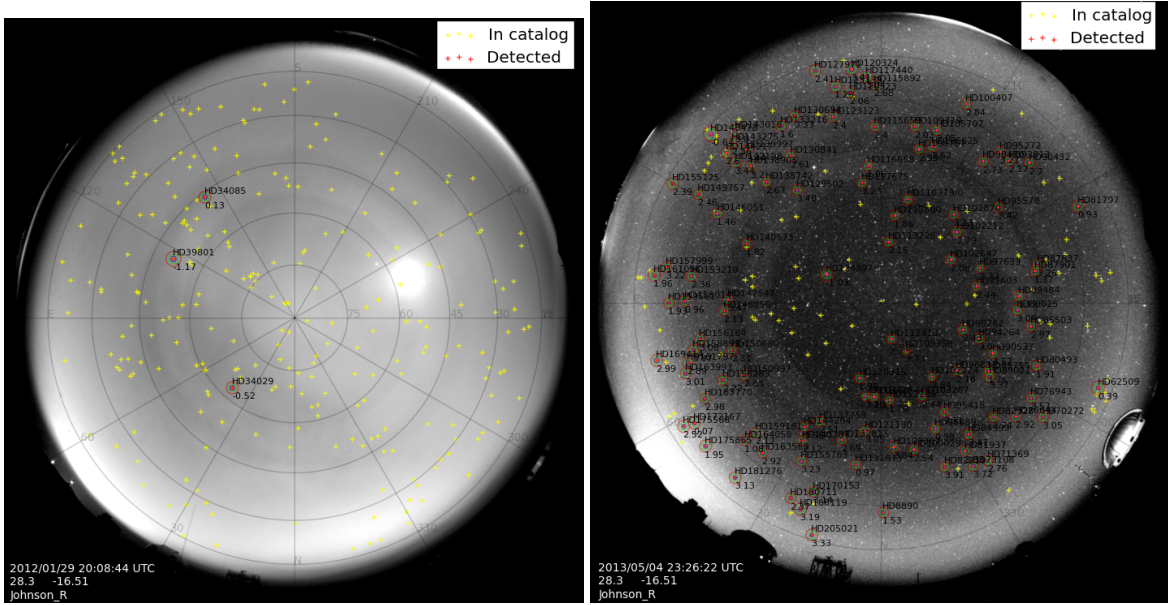


FIGURE 3.3: Comparison between a hazy (left) and clear (right) night in the star detection process. Note that only the Moon, Jupiter and the brightest stars can be seen in bad conditions. In contrast, we can detect more than 100 stars in a single frame if the night is clear.

An obvious future improvement in this direction would be to implement an automatic image field solver (just like *astrometry.net*⁴), but since fisheye lenses tend to distort the field at high zenithal angles, this should be done carefully.

The details of the star detection algorithm were presented in [13]. The algorithm is essentially the same used in this work, but with some changes in the detection threshold and performance improvements. Basically, the star position is computed from the catalog equatorial coordinates and the astrometric solution, the calculated position is optimized with a centroid calculation and some checks are performed to be sure that the star has been really detected.

To perform the instrument calibration, only stars with good photometric properties can be used. Thus, we discard every double or variable star from the detected star list and also those with bad (saturated/cold) pixels in the image.

Then, we have to use the measured star fluxes on the image ($F(c/s)$) and the catalog magnitudes (m_0) to calibrate the instrument zero point and atmospheric extinction. This is done fitting the photometric data to equation 3.4[14]:

$$m_{\lambda,0} + 2.5 \log_{10}[F_{star}(c/s)] + \psi_{\lambda}(m_{\lambda,0} - V) = C_{\lambda} - K_{\lambda}\chi \quad (3.4)$$

with $m_{\lambda,0}$ the star tabulated magnitude, $F_{star}(c/s)$ the measured flux in the image, C_{λ} the instrumental constant, K_{λ} the atmospheric extinction, χ the air mass and ψ_{λ} the color term, that multiplies

⁴We have already contacted Dustin Lang, one of the authors of *astrometry.net* at Princeton University to discuss the possible implementation of different field projections in their software.

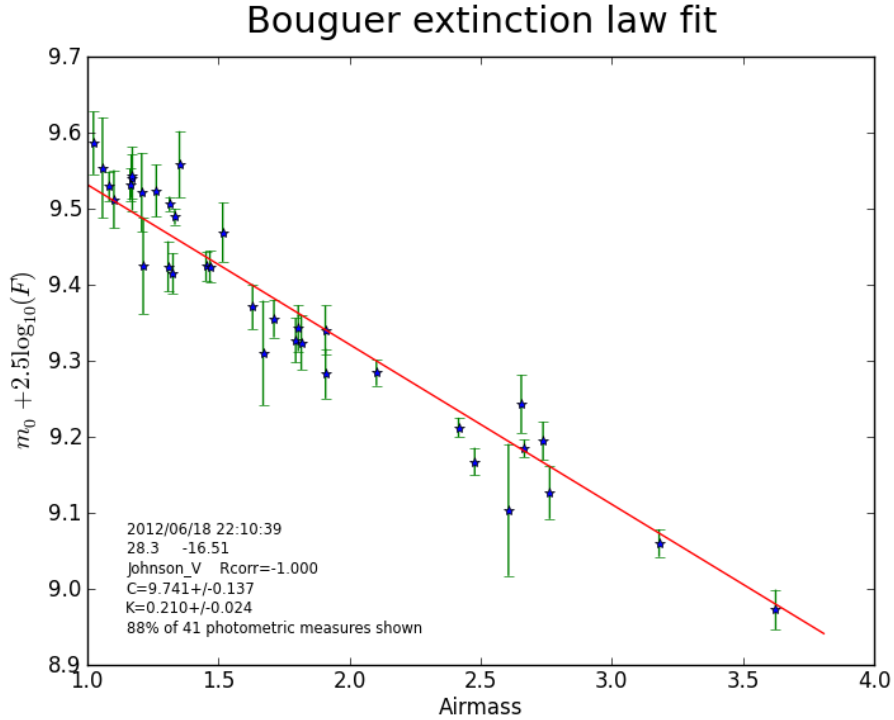


FIGURE 3.4: Example of Bouguer extinction law fit done with PyASB.

the color $m_{\lambda,0} - V$. The simple air mass estimation $\chi = \sec(z)$ of the plane-parallel atmosphere solution is no longer valid since we are extending our measures up to $z \sim 75^\circ$ (air mass $\chi \sim 4$). We use instead the more accurate interpolation formula from [15].

Once the instrument constant is calculated, we take the background flux (median of background pixel values that do not contain bright stars) and convert it to Night Sky Background brightness (NSB) with the equation:

$$NSB_\lambda \text{ (mag/arcsec}^2\text{)} = C_\lambda - 2.5 \log_{10} \left[\frac{F_{NSB}(\text{counts})}{N(\text{px}) \times t(\text{seconds}) \times A(\text{arcsec}^2/\text{px})} \right] \quad (3.5)$$

Finally, the cloud detection is done using a star counting method around the field. This can be done binning the sky in regions and counting how many stars we expect to be detectable for the given sky parcel and how many of them have been actually detected. Another option is to perform the same relative star counting process for the complete field and then giving a ‘mean’ cloud coverage fraction for the whole sky. In the long-term analysis of Izaña data, we have used only the wide field data (down to $z \sim 60^\circ$) to speed-up the process.

Note that the detectable star percentage is a robust but a bit simplistic proxy to the mean cloud coverage. There may be stars in the field that cannot be detected due to stochastic issues (p.e., a dust spot in the dome, a bad astrometric solution of the field, a bad pixel or a misbehavior of the optical system because of dew).

At the same time, we may have a little amount of false stars detected (cosmic rays, reflections in the dome of a powerful light source such as the Moon or city lights). This introduces a bias in both the

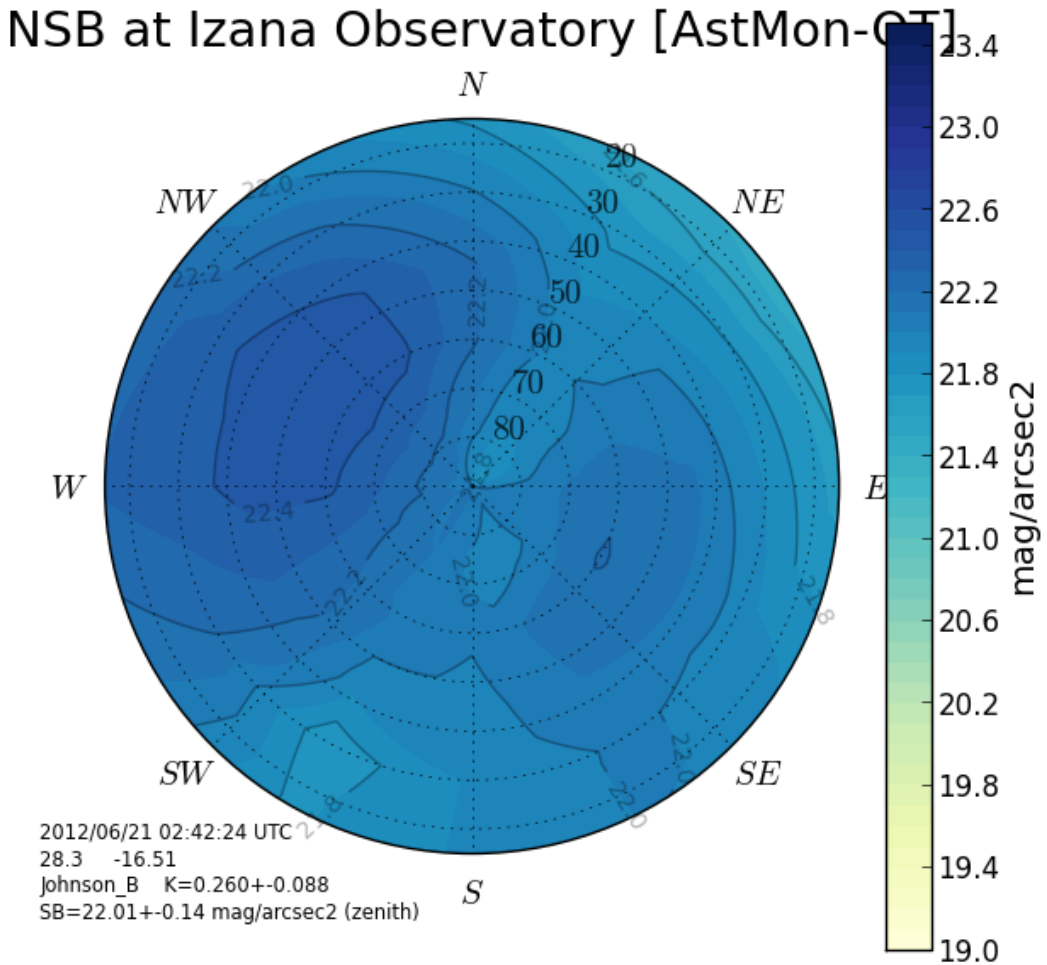


FIGURE 3.5: B-band sky background map at Izaña’s observatory. The Milky Way is crossing the zenith.

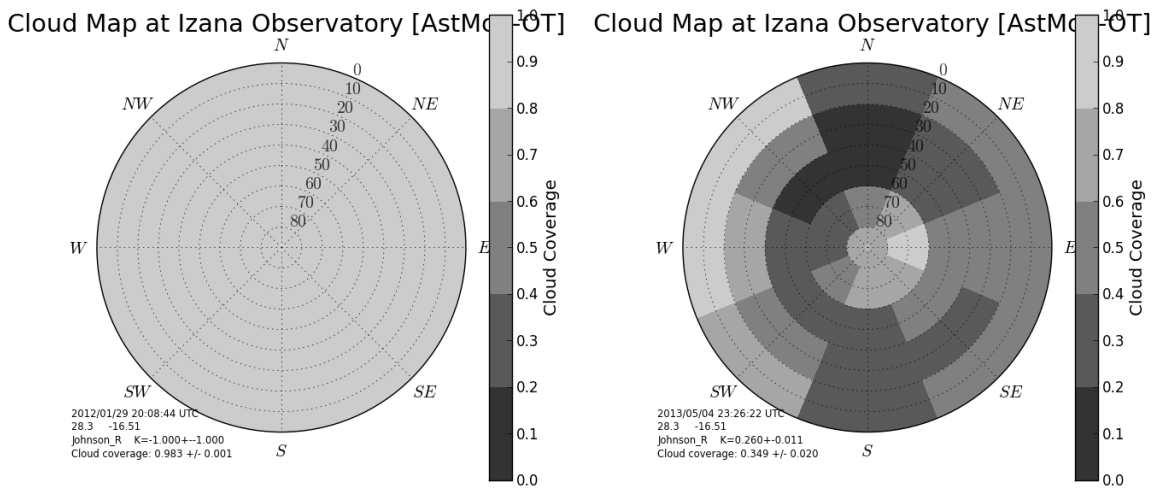


FIGURE 3.6: Comparison between cloudy (left) and clear (right) nights in the cloud detection process. It is clear that an all-sky camera equipped with a fisheye lens can serve as a robust cloud detector, very useful for remote observations with robotic telescopes. However, fine tune-up for each system is needed to correctly estimate the cloud coverage with star detection percentage.

minimum stars (at overcast) and the maximum stars in a completely clear night that should be taken in the future versions of the algorithm.

We tried to reduce these biases looking at cloudless images and images with an overcast sky and optimizing the detection thresholds, but there is still a number of stars that will not be detected because other issues (p.e. high proper motion).

If one also wants to differentiate between cloud types (lets say, point out if we have cirrus/high altitude clouds that simply affect the average transmission of the atmosphere or low clouds that are optically thick), this proxy should be tuned with other indicators such as the extinction. Thus, the next step in this direction would be to produce extinction maps.

3.2.3 Data Output

We have already presented some plots generated with the PyASB image analysis process. We note that the data is also provided as text/table files with the photometric measures for detected stars, the measured night sky background and cloud coverage at different directions.

Finally, a summary file for each image is produced with information about the quality of the photometry, the measured zero point of the system, the mean extinction coefficient, the night sky background at zenith and the mean cloud coverage.

The set of summary files produced by the analysis of large data series will be subject of further analysis in Chapter 4.

3.3 Long-term data analysis

The image analysis pipeline is very productive to analyze the sky conditions at a given date and time, but most of its results are variable over time. If our goal is to study the mean sky quality conditions in the site, we would need to make long-term statistics to remove the outliers and short-term variations in the data.

In order to make the statistics, we have collected AstMon data at Teide Observatory from February 2012 to May 2013 (the operators of the instrument did some tests with the device on January 2012 and the results for this month are a bit inconsistent, so they have been removed from the analysis). This time period translates into $\gtrsim 18000$ images that have been analyzed with PyASB in two phases (the first was a calibration run to obtain the instrumental constant of the device, the second phase was the fine analysis of the data with a fixed instrumental constant justified because we have not detected any long-term evolution of this parameter).

The complete analysis is time consuming because of the way we do the night sky background and cloud coverage measures (we divide the sky in sectors and make statistics on each sector) and the large list of images to analyze. Since we have some time constraints for this work and the Izaña's site characterization in the CTA context (the deadline to provide data is June 30), we opted to make a short analysis, obtaining only the zenithal sky background and the mean sky coverage from zenith to

$z \sim 60^\circ$. The result of this analysis is a set of “summary” files, that will be processed with the PyASB summary analysis pipeline.

This analysis module consists on a python script with separate functions to perform each single operation we want to do on the data, from obtaining the mean of extinction coefficients with a filter to fitting the galactic effect on the night sky background with a functional curve or to make histograms on the cloud coverage values. As a result, several plots and fit summary files are generated.

PyASB’s scripts can also operate with data from different filters and match their data (remember that the camera is monochrome, so there is a small offset in the raw image timestamp between images in different filters, which complicates the color analysis).

In the following chapter, we present the main results of the long-term analysis at Teide Observatory using this module.

Chapter 4

Results

4.1 Izaña site characterization

The Cherenkov Telescope Array project (CTA hereafter) will be the next generation of ground-based Very High Energy gamma-ray instruments. It has a wide range of applications in astrophysics and it is expected to provide the main clues of the non-thermal high-energy universe.

The Cherenkov Telescope Array will count with two observatories, one in the southern hemisphere to study mainly the Galactic sources (and put constraints on the Dark Matter at the Galactic Center) and the other at the northern hemisphere to study mainly extragalactic sources such as AGNs and GRBs.

The CTA consortium is currently looking for places to install both observatories. At the Northern hemisphere, the candidates are San Pedro Mártir (Mexico), Meteor Crater (USA) and Izaña (Spain).

The CTA consortium has started several meteorological and night sky quality campaigns in these sites in order to be sure that the best site is selected for the project. In that sense, the author of this thesis has been involved with the Spanish CTA group in the Izaña's site characterization, collaborating with the AstMon-OT data and measures from a SQM photometer we installed at Teide Observatory last summer.

4.2 Night Sky Background

In order to summarize the results of the night sky background study, we present in (4.2) the histogram of measures for the given AstMon filters at Teide Observatory. As seen from these graphs, the



FIGURE 4.1: Artist impression of the Cherenkov Telescope Array at Izaña.

	k_B	k_V	k_R
Kidger et al. 2006. (<i>mag / airmass</i>)	$0.220^{0.133}_{0.042}$	$0.132^{0.144}_{0.058}$	$0.098^{0.157}_{0.045}$
AstMon-OT (<i>mag / airmass</i>)	$0.351^{0.071}_{0.071}$	$0.246^{0.122}_{0.090}$	$0.215^{0.085}_{0.071}$
Difference (<i>mag / airmass</i>)	~ 0.131	~ 0.114	~ 0.117

TABLE 4.1: Comparison of AstMon-OT data with Kidger measured values of extinction at Canary Islands' International Observatories (uncertainties are derived using the decile values from Table II on Kidger 2006). In AstMon, we use also the deciles.

distribution peaks at ~ 22.4 , ~ 21.3 and $\sim 20.7 \text{ mag/arcsec}^2$ with a small tail of very dark nights and a larger tail of worse nights.

As seen from (4.3), some intrinsic dispersion is found in the data from night to night and through a single night due to changes in atmospheric conditions.

There seems to be also a seasonal variation in this parameter (4.4a). This may be attributed to changes in the dominating atmospheric flows along the year. In summer, the Atlantic winds tend to be weaker than in Winter. This makes it easier for Saharan winds to reach Canary Islands, bringing desert dust (aerosols).

Autumn and Spring should be considered as transitional seasons. Depending on the importance of each of the effects we mentioned early, some changes in the mean night sky background are expected.

Light pollution typically evolves over the night due to the slow turn-off of city lights. This process continues until a stable value is reached (typically at 12pm-2am, local time). Fortunately, Izaña is a reasonably dark site at high altitude and the effect of this human activity at cities is not as important (4.4b) as in heavy polluted sites like UCM's urban observatory¹.

4.3 Extinction

We can obtain with PyASB plots for the extinction parameter similar to those we have shown for the sky brightness. We should remark however that the atmospheric extinction is a difficult variable to track because it requires a scrupulous calibration of the photometric system.

In our case, we have already argued that we are not sure if the vignetting of the system is well characterized in AstMon all-sky camera. Looking at the mean extinction values we obtained here for photometric or nearly-photometric nights[4.1][4.5] and comparing them with the values quoted in the bibliography for the Canary Islands observatories[16][17], there are clear evidences that this might be affecting our data.

One strong argument in favor of this idea is the fact that the difference of our calculated extinctions and those from the Bibliography is essentially the same (between $0.110 - 0.130 \text{ mag/airmass}$) for the three bands[4.1].

Another question we may ask is if there is a change in the extinction between seasons. In that sense, we expect a higher values (particularly in R and V bands) in summer due to the increasing amount of Saharan dust (aerosols) in the atmosphere. We see in Figure (4.7) that, as expected, there is an evident

¹See Appendix A.1 for further details

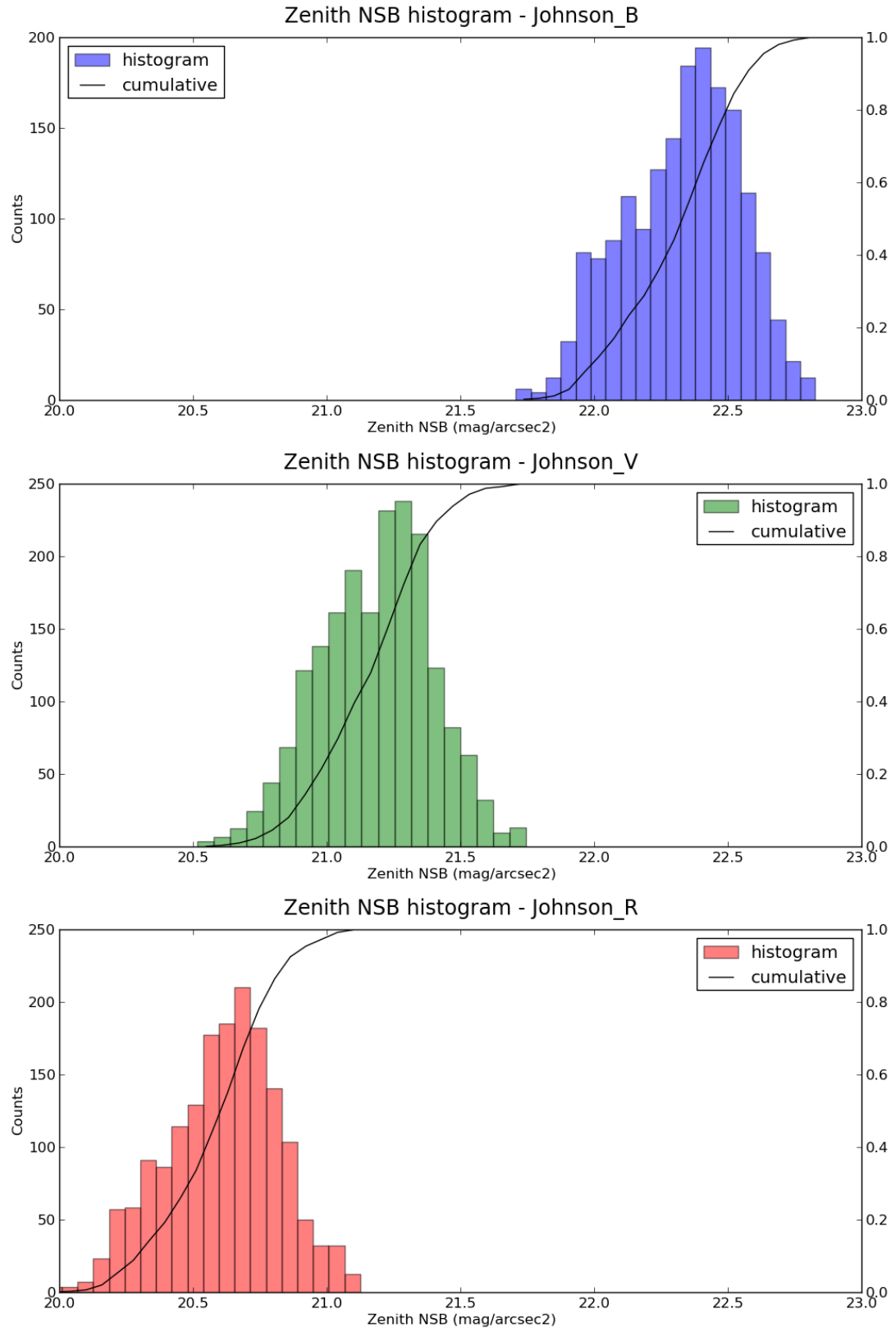


FIGURE 4.2: Zenithal Night Sky Brightness histogram measured with AstMon-OT.

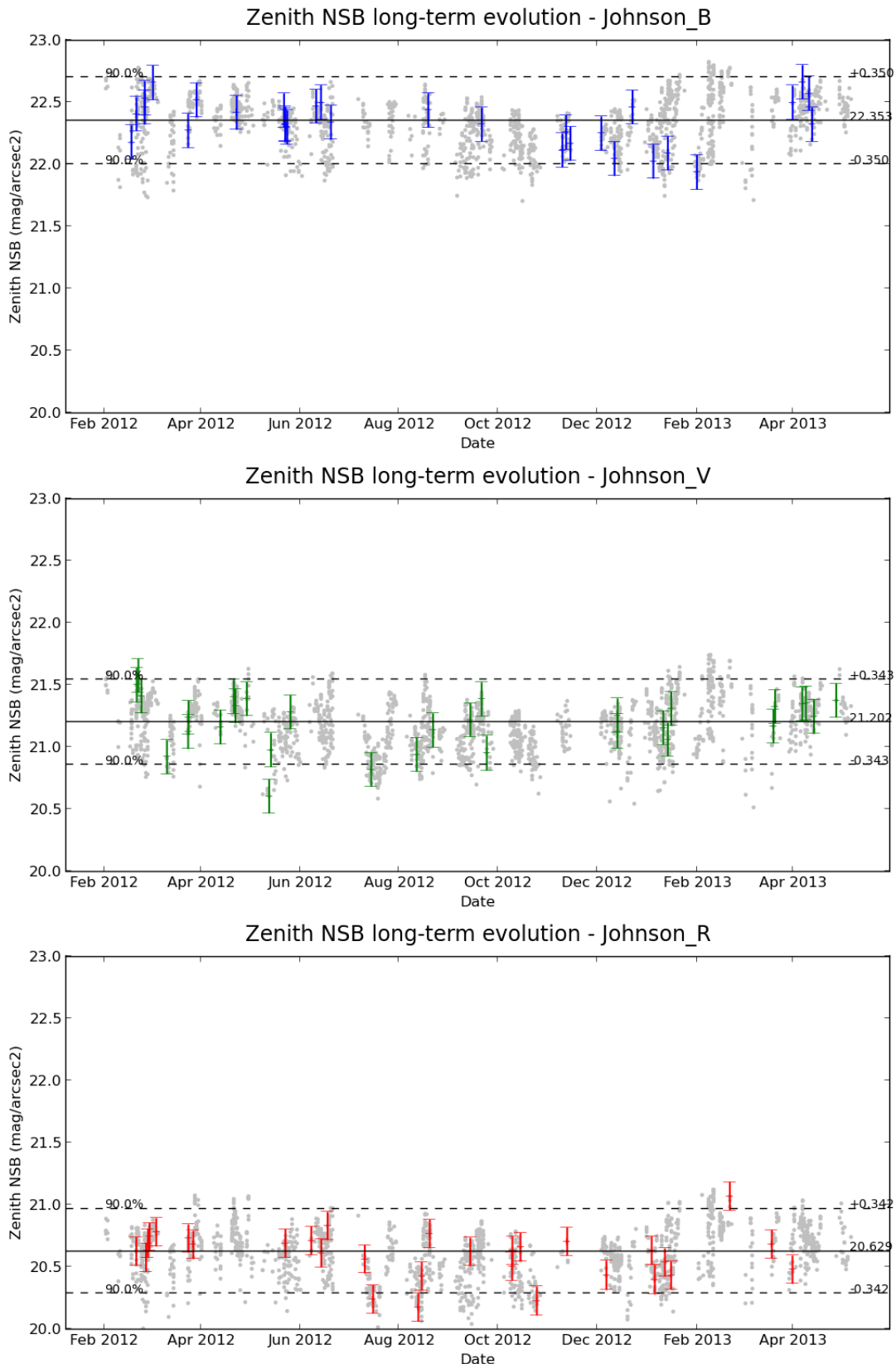


FIGURE 4.3: Zenithal night sky background evolution over the time from AstMon-OT. Only clear nights are shown. The median and the interval that contains the 90% of the data is given. To improve readability, only some error bars are plotted.

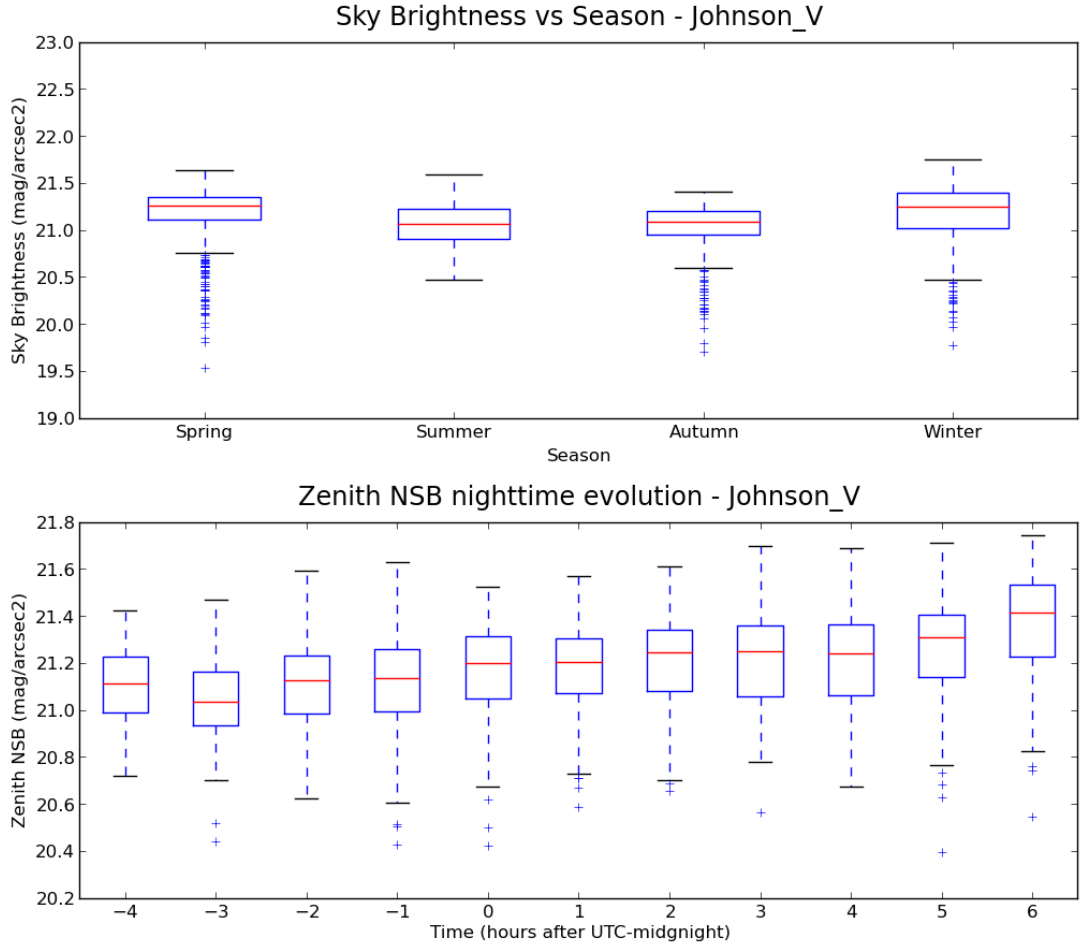


FIGURE 4.4: **Upper graph:** Seasonal changes on the night sky background in Johnson V at Izaña.
Lower graph: ‘Average’ night sky background evolution over the night.

In both graphs the boxes represent the 1/4 quartile, the median (red line) and the 3/4 quartile. The error bars represents the limits of the data (not counting outliers).

	U	B	V	R	I
$\bar{\lambda}(\text{\AA})$	3663	4361	5448	6407	7980
$\Delta\lambda(\text{\AA})$	650	890	840	1580	1540

TABLE 4.2: Effective (mean) λ s used in extinction slope-slope diagrams [2]. A better estimation of this effective extinction weighted- λ for each AstMon band should be considered in the future, but for our purposes this simple mean estimation is enough.

effect of aerosols in summer. Extinction values are clearly higher at this season and lower at winter, when the Atlantic flows (wetter, without dust) dominate.

This can be stated also if we calculate the slope of the extinction parameter. If the extinction is dominated by a Rayleigh law, then one expects

$$\frac{K_B}{K_V} \propto \left[\frac{\lambda_B}{\lambda_V} \right]^{-4} \rightarrow \log \left(\frac{K_B}{K_V} \right) \propto -4 \log \left(\frac{\lambda_B}{\lambda_V} \right) \quad (4.1)$$

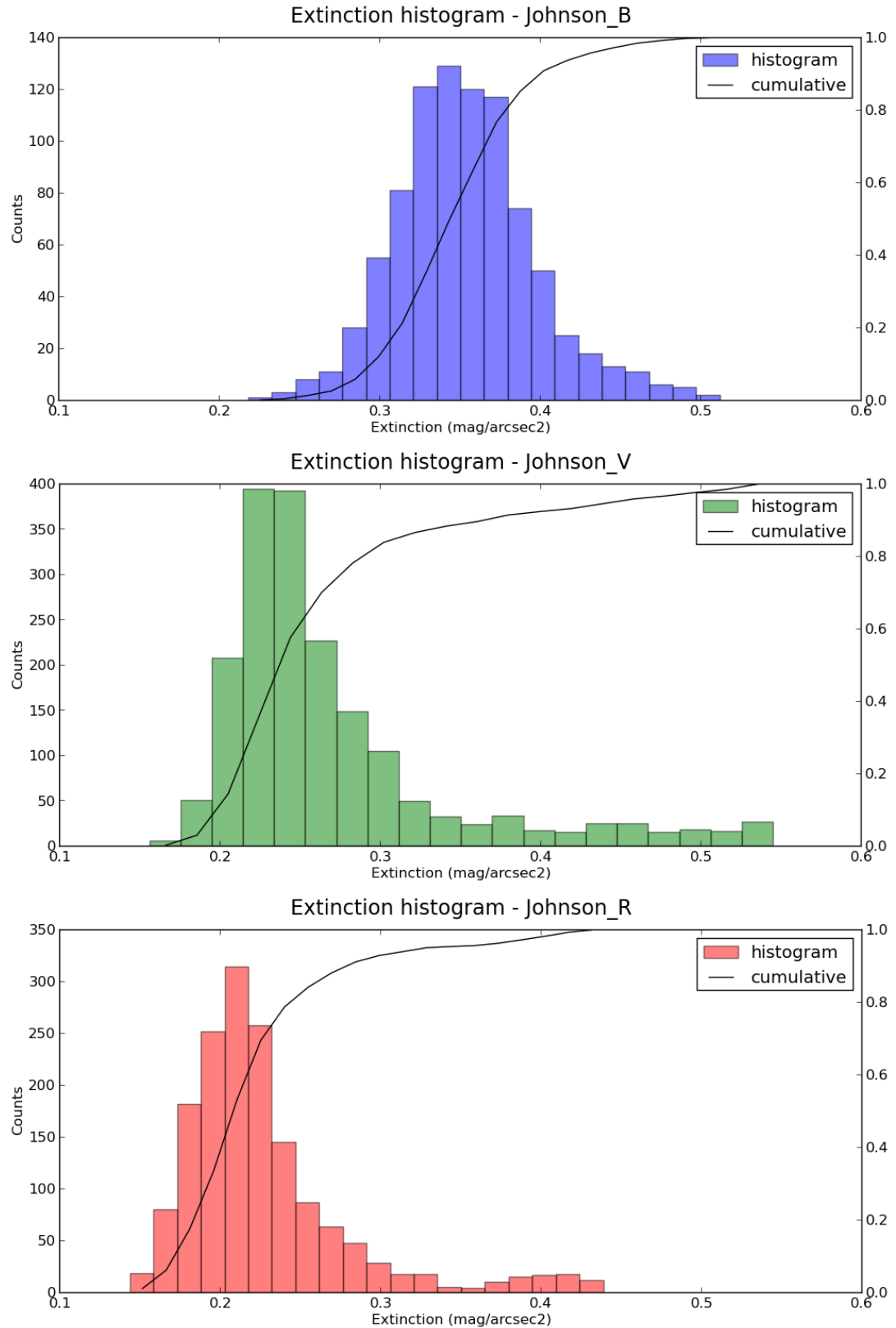


FIGURE 4.5: Measured extinction values found at Izaña. Only cloudless images are shown.



FIGURE 4.6: Saharan dust as seen from satellite images.

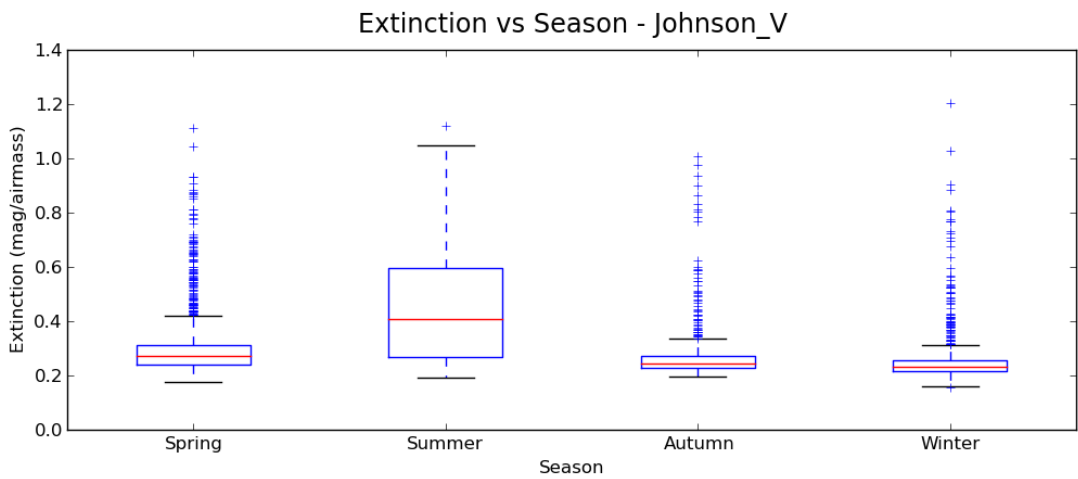


FIGURE 4.7: Johnson V extinction values found at Izaña, averaged within seasons. As with the NSB nighttime evolution, the boxes limits and red lines represent the quartiles and the median, whereas the errorbars shows the data limits (excluding outliers).

In the majority of nights, however, there will be an extra component from dust and aerosols that dismiss the significance of this relation. In other words, the extinction will be more similar between filters. A simple way to classify nights by their aerosols concentration is then to simply plot a ‘ratio-ratio’ diagram with two different filter pairs. We assumed the effective wavelengths given in table (4.2).

From (4.8) we see how nights with high atmospheric concentration of aerosols differ in extinction from clear nights. A weak sky color dependence is also found with the aerosol concentration.

4.4 Cloud coverage

Another subject of interest is to follow the cloud coverage evolution at the observatory. This is particularly interesting in order to make statistical estimates of the usable nights for astronomical observations and also to remove undesirable measures of night sky background and extinction in our analysis.

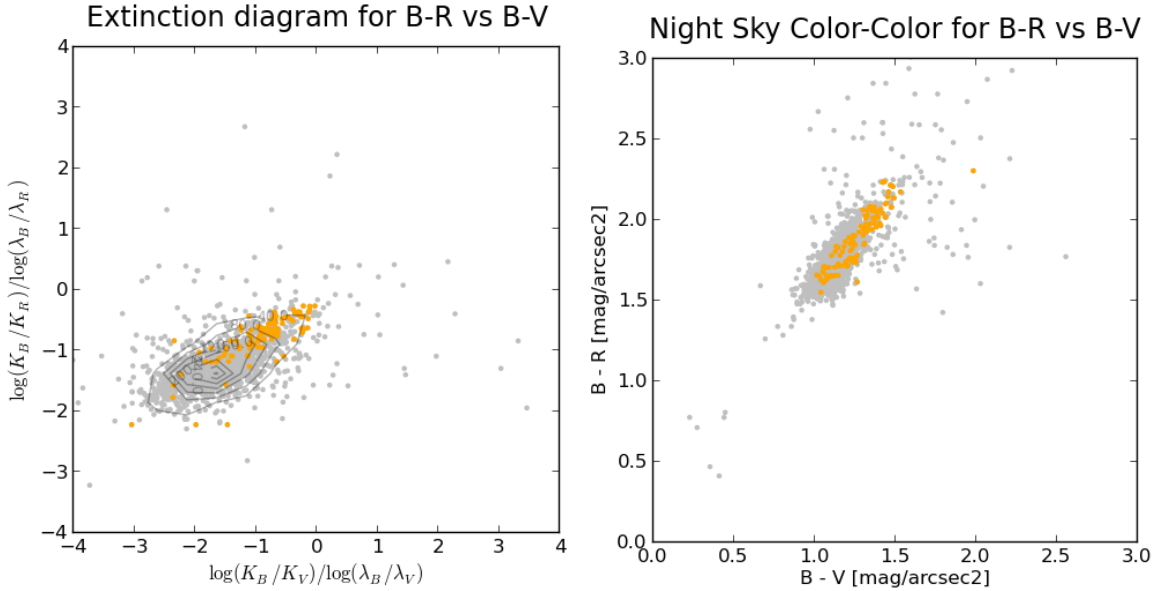


FIGURE 4.8: **Left:** Extinction slope-slope diagram for AstMon-OT. July 2012 data (a exceptional case with nearly no aerosol-free days) is marked in orange. **Right:** Color-color diagram for AstMon-OT. July 2012 data is also marked in orange.

Figure 4.9 characterize the measured cloud coverage at Teide Observatory for the range of dates under study. We must emphasize that we are using a star counting method for the cloud coverage estimation, that simply represents the percentage of stars that are detectable in the image (if the cloud coverage index increases, then less stars are visible in the sky).

We have seen that this cloud estimation has an offset with respect of the fraction of detected stars at the low end limit (we loose systematically around 10% of stars). We fixed it by doing a clipping of the data between the 5% and 95% percentiles, assuming that these tails corresponds to completely clear and overcast nights. Figure 4.9 shows the cloud data corrected from this bias.

The histogram is clearly bi-modal with some points located at intermediate cloud index values that represents, in the majority of cases, nights with aerosols or Saharan dust that do not let us to see faint stars. If we suppose that nights with a ‘cloud coverage index’ below $\sim 1/3$ are in fact clear nights, then one can point that the number of clear nights is in the order of 75%.

From (4.9), we see that Izaña has a high percentage of clear nights. This is easily understandable if one takes into account that the main source of clouds at Canary islands is the trade winds.

These trade winds (‘Alisio’) bring clouds to Tenerife and La Palma that are normally at low altitudes, typically below the observatory altitude. Their effect is commonly known as the ‘Sea of Clouds’ and, in fact, it helps to lower the light-pollution effect by reflecting downward the light from cities. Some previously done studies carried by Rafael Barrena and Miguel Nievas at IAC show that this effect can effectively darker the sky in $\sim 0.1^{mag}$ in V band[18].

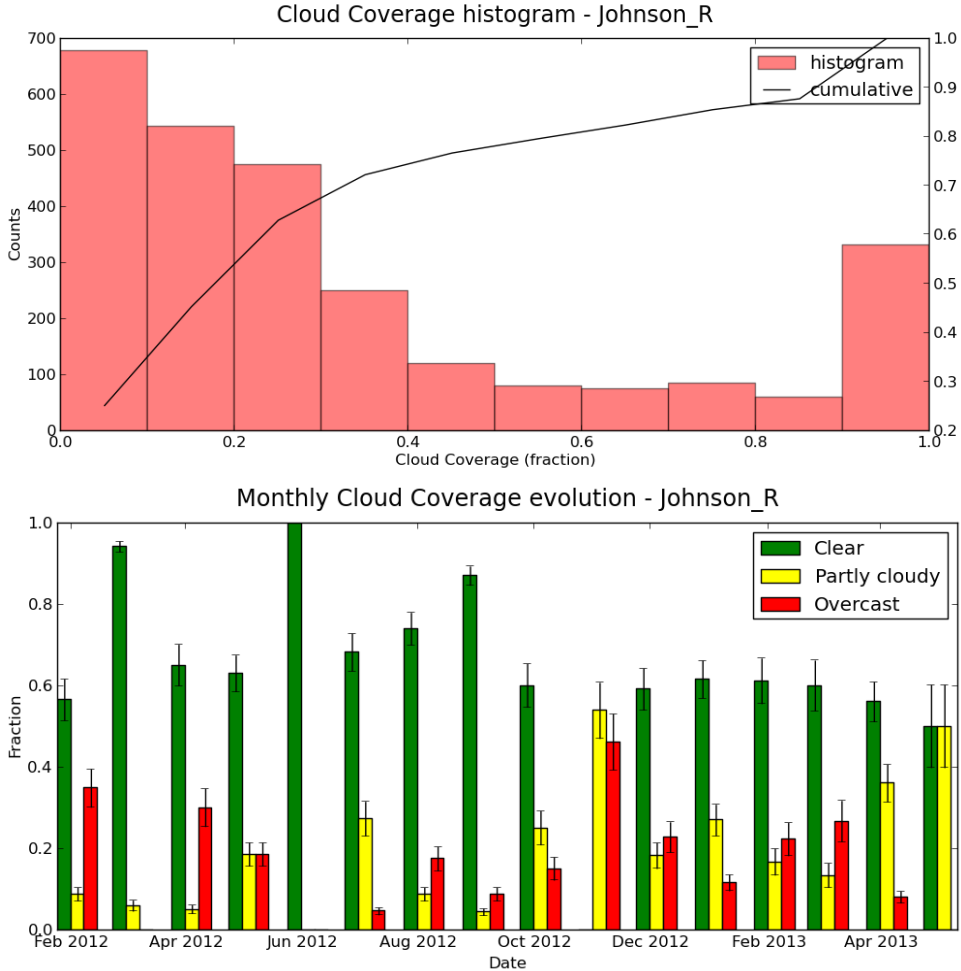


FIGURE 4.9: Cloud coverage histogram at Teide Observatory.

	B	V	R	I
IAC80-OT ($\text{mag}/\text{arcsec}^2$)	22.34 ± 0.25	21.23 ± 0.33	20.43 ± 0.20	19.36 ± 0.23
ORM* ($\text{mag}/\text{arcsec}^2$)	22.70 ± 0.03	21.9 ± 0.03	21.0 ± 0.03	~ 20.0
diff OT-ORM ($\text{mag}/\text{arcsec}^2$)	0.36 ± 0.24	0.67 ± 0.13	0.57 ± 0.21	~ 0.64

TABLE 4.3: Median of Night Sky Background taken with IAC80-OT in the sky quality routine observations of the IAC. Comparison with values for Roque de los Muchachos taken at Isaac Newton Group is shown (<http://www.ing.iac.es/Astronomy/observing/conditions/skybr/skybr.html>).

4.5 Comparison of AstMon data with IAC80

Support Astronomers of IAC have collected Night Sky background images for Johnson-Cousins B, V, R and I bands with the IAC80 telescope in a campaign that lasted from March 2011 until July 2012. These images have been analyzed by Rafael Barrena and Miguel Nievas and there are plans to publish them soon.

As seen from 4.3, Teide Observatory is not as dark as Roque de los Muchachos Observatory, but clearly better than the light-polluted skies of Madrid. With IAC80, we can easily check the results obtained with AstMon-OT. The comparison of IAC80 and AstMon-OT is summarized in table 4.4.

	B	V	R
IAC80-OT ($mag/arcsec^2$)	22.34 ± 0.25	21.23 ± 0.33	20.43 ± 0.20
AstMon-OT ($mag/arcsec^2$)	22.35 ± 0.35	21.20 ± 0.34	20.63 ± 0.34
AstMon-OT [color corr.] ($mag/arcsec^2$)	22.33 ± 0.35	21.20 ± 0.34	20.43 ± 0.34

TABLE 4.4: Comparison of our AstMon-OT measures with IAC80 Night Sky Background data.

From 4.4, we find some differences between AstMon and IAC80 in R band. This is probably due to the spectral response of the former, that seems to be a bit different to the standard Johnson R filter band. This effect can also be seen in AstMon-UCM data and AstMon-CAHA².

During the calibration process done in AstMon-OT, we found a tentative value for the color correction in R band of $\psi_R \cdot (R - V) = (-0.3443 \pm 0.0050) \cdot (R - V)$, where ψ_R is the color term. If we correct AstMon-OT data with this color term (see last row of 4.4) using the mean R-V for OT skies, then the NSB at R band adopts a value of $20.43 \pm 0.34 mag/arcsec^2$, which is similar to IAC80's. The same procedure can be done with B filter. In this case, the correction is $\psi_B \cdot (B - V) = (0.02154 \pm 0.0073) \cdot (B - V)$ and the corrected NSB is, thus, $22.33 \pm 0.35 mag/arcsec^2$. From these results, it turns clear that color correction terms are very important to obtain correct values for the Night Sky Background with all-sky cameras, so these color terms are good candidates for further analysis in the future. In the meantime, we decided to use the raw (color-uncorrected) data in the analysis.

We must point however that it is not necessary for the measures taken with different instruments to completely agree since they have been collected at different epochs and conditions (many telescope measures published in the bibliography are referred to pre-filtered dark and moonless nights, without the Milky Way present. On the other hand, we are working with the raw mean values for just all acceptable nights based on cloud measures from the same instrument).

4.6 Moon effect on the night sky background

The effect of the Moon in the night sky background has been studied for a long time[20][21] and its modeling[22][23] has important applications in exposure calculators, widely used in astronomical observatories. The Moon effect is more or less important depending on the type of astronomical observation.

In compact sources the increasing background level does not critically increment the background noise of the data. On the other hand, if the subject of interest is an extended and low surface brightness object, the increase of only $0.5 mag/arcsec^2$ in the sky background can make a difference between detecting the source or loosing it in the noise.

In Cherenkov astronomy it is common to rule out observation nights with moonlight because of the night sky background increase, which limits the quality of the data. This, for example, limits the duty cycle per year of the MAGIC telescopes to $\sim 12\%$ (between astronomical dusk and dawn and with the Moon below the horizon).

²See [19]

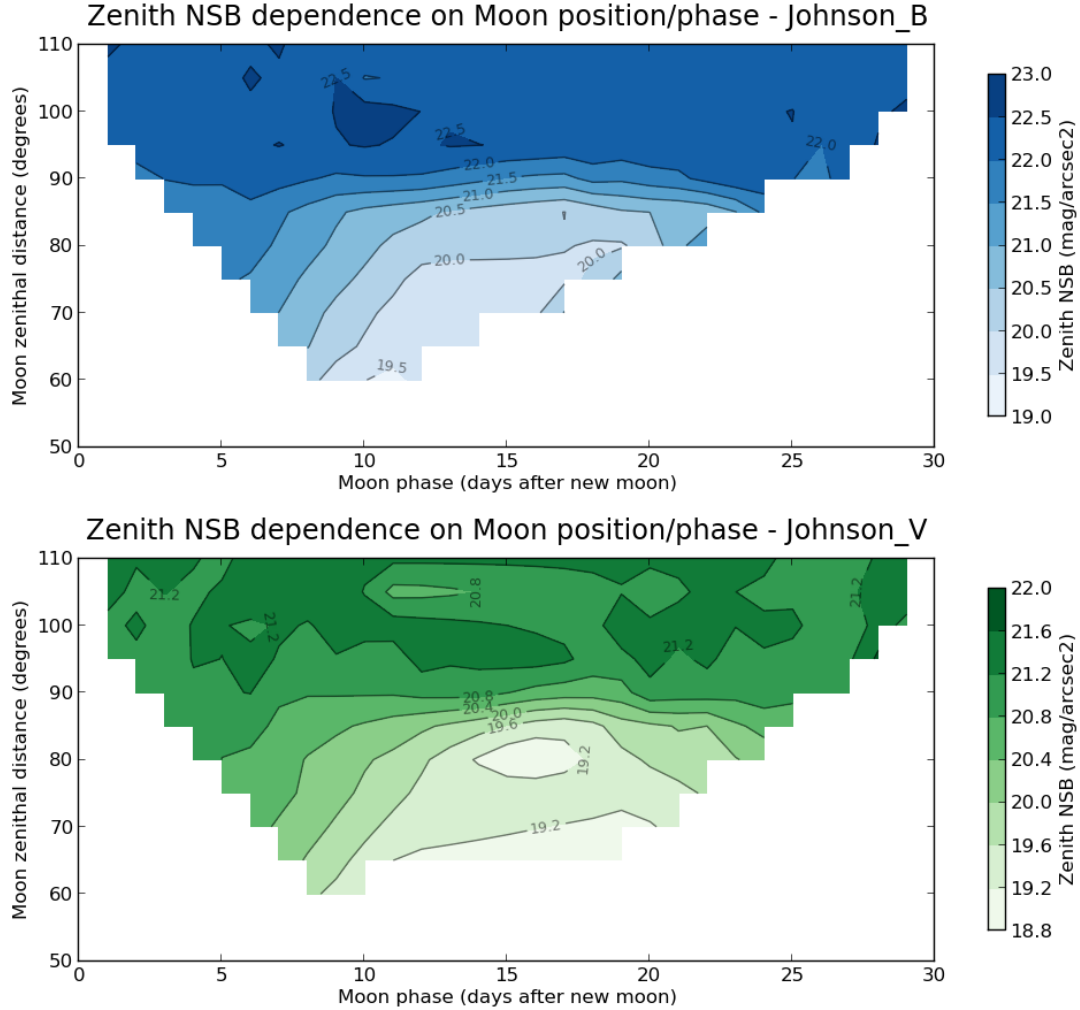


FIGURE 4.10: Moon position and phase effect in the zenithal night sky background. The first two graphs refers to Johnson B and V measures. The bottom is a composed B-V map.

Some studies[24] however point that relaxing this requisite could increase the duty cycle to nearly a $\sim 18\%$ (up to 1500 hours of observation). Some tests done at the Whipple collaboration (VERITAS, Arizona) limiting the PMT working range to the UV with filters or at HEGRA experiment with reduced gain on the PMT dynodes show that it is possible to observe in gray nights with only a minor degradation in energy thresholds.

With AstMon we have an exceptional opportunity to study the effect of the Moon in night sky background at different photometric bands. Its future application in the optimization of Cherenkov observations seems to be evident.

If we restrict our attention to only zenithal data, the main two variables that could change the effect of the Moon in the sky background are the Moon altitude and the Moon phase. They are clearly correlated, because the Moon phase determines how high can get the Moon at nighttime (new Moon reaches its highest altitude at daytime), so we will not try to analyze them separately.

Instead, we present a contour plot in Figure 4.10 with the Moon phase in X axis and the Moon zenithal distance in the Y axis. The color gradient represents the NSB in $mag/arcsec^2$ at zenith.

As we see, the (full-)Moon effect is quite different between photometric bands. In Johnson B, the increase in night sky background can be as high as 3.0 mag/arcsec^2 (from a value of $\sim 22.5 \text{ mag/arcsec}^2$ with no Moon to $20.5 \text{ mag/arcsec}^2$ with Moon at $z \sim 80^\circ$ and $19.5 \text{ mag/arcsec}^2$ at $z \sim 60^\circ$). The situation could be even more dramatic if we had measures in AstMon-OT with higher Moon altitudes, but the AstMon capture program stops taking data when the Moon is high above the horizon.

In V band, the change is lower, $\sim 0.8 \text{ mag/arcsec}^2$ between $z > 90^\circ - 80^\circ$ and $\sim 2.0 \text{ mag/arcsec}^2$ up to $z \sim 60^\circ$, but is also noticeable.

The difference between B and V bands implies a change in the sky color, the Moon makes the sky bluer. This is important because it explains why in ‘bright nights’ (with Moon above the horizon), it is preferred to observe in near-infrared bands. In them, the Moon is not as bright as in visible and also the sky is already bright because of the atmosphere.

Because of the large contribution of the Moon to the night sky background, we have been forced to restrict the analysis of AstMon-OT data to moonless nights.

4.7 The Milky Way effect on the night sky background

The Galactic light is responsible of an important amount of background photons in some regions of the sky. The sources of this background flux are mainly individual unresolved stars, ISM scattered light and emission from extended sources like nebulae.

The first source of light can be partially avoided by using instruments with enough spatial resolution. In that sense, measures with CCD and telescopes will be always preferable over measures with a SQM photometer ($FWHM \sim 20^\circ$). With CCDs, we can resolve some of the brightest stars in each field and then avoid contaminating the background with their fluxes. With AstMon however, the resolution is quite coarse. This greatly reduces the amount of stars that can be identified in the field (e.g. $V \lesssim 6^{mag}$).

Figure 4.11 shows the measured sky brightness dependence with the galactic latitude. In order to give a simple model of the effect of the MW, we fit the data to a Gaussian law,

$$NSB = a + b \cdot \exp \left[-\frac{(x - c)^2}{2d^2} \right] \quad (4.2)$$

This does not answer any physical reason, but only the fact that the Galactic plane has a limited height scale. Beyond its limits, the night sky background should be nearly flat if we do not consider other effects.

A Gaussian fit seems also interesting because it gives directly some precious magnitudes such as the height scale of the Galactic plane ($d \sim FWHM$), the depth of the curve (the greatest brightening that can be induced by the presence of the Milky Way, b) and the non-contaminated mean level of the night sky background (a). The parameters of this fit are given, for each filter, in Table 4.5.

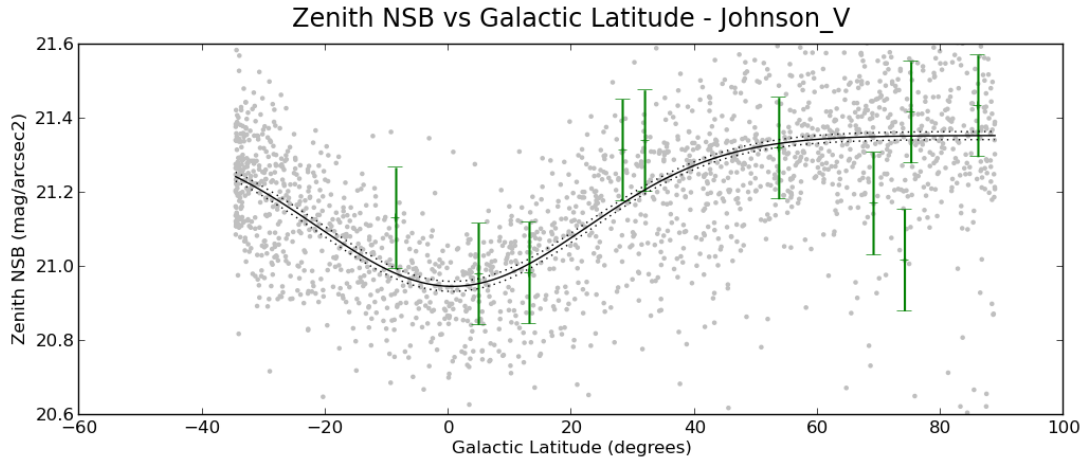


FIGURE 4.11: Milky Way effect in different photometric bands.

Filter	a ($\text{mag}/\text{arcsec}^2$)	b ($\text{mag}/\text{arcsec}^2$)	c (deg)	d (deg)	χ_{red}	N_{data}
B	22.516 ± 0.047	-0.503 ± 0.075	0.4 ± 2.9	21.5 ± 3.9	0.010	1603
V	21.353 ± 0.047	-0.407 ± 0.069	0.6 ± 3.4	21.9 ± 4.6	0.014	1751
R	20.737 ± 0.041	-0.413 ± 0.076	0.0 ± 3.3	17.5 ± 3.9	0.015	1540

TABLE 4.5: Parameters of the Milky Way effect model on the night sky background.



FIGURE 4.12: Airglow as seen from the ISS spacecraft.

This analysis let us to easily predict how many Galactic photons are contributing to our local sky background at a given position in the sky, which is important for noise and SNR (signal to noise ratio) calculations.

4.8 Other effects

There are other known sources of light that may affect our data. One of such sources are the solar activity that may brighten the upper atmospheric layers through the ionization and excitation of atoms like Nitrogen or Oxygen. This effect is commonly known as ‘Airglow’ (see Figure 4.12), and should be more pronounced when the Sun is more active and in high magnetic latitude sites.

Some studies have found that airglow and zodiacal light (another contribution to the night sky background caused by dust in our solar system) are the main sources of natural light in the sky. This encouraged us to try to see both effects with AstMon-OT, being aware that our study would probably not be sensible enough as we are looking only into a narrow field around the zenith.

In this sense, we expect the airglow effect to be larger on high zenithal angles due to the thicker atmosphere depth. On the other hand, the zodiacal light is brighter near the ecliptic plane and near the twilights, but AstMon is only observing at astronomical night, far away from these twilights.

To study the airglow, we tried to plot the night sky background vs the solar radiance at XUV (in steps from 1Å to 1216Å) using the *Solar Dynamics Observatory* data from http://lasp.colorado.edu/eve/data_access/evewebdata/quicklook/L0CS/SpWx/. In the case of the zodiacal light, we tried to see if sky background varies with the ecliptic latitude.

In both cases, we found no evidence of variations of the night sky background due to these effects. This can be explained probably because AstMon, in its actual working state, is not optimized for this type of observations. There is also the fact that zodiacal light and airglow might be subdominant in front of larger effects such as the atmospheric conditions and the Milky Way. We may expect that the modeling of stars and Galactic contributions would help to study these secondary effects.

Chapter 5

Conclusions

All-sky cameras are promising instruments for site testing because of their ability to make measures with spatial and temporal resolution. This allows us to study time and spatial dependency of night sky quality parameters such as the night sky background, extinction coefficient and cloud coverage.

We have pointed that all-sky cameras have important caveats. In order to work as expected, they need a exquisite calibration of system response, saturation point of the CCD, vignetting of the optical system and the CCD dark current and bias. In that sense, we remark how difficult is to generate a perfect flat field for an all-sky instrument and how easily a bad flatfield can lead us to incorrectly estimate the instrumental constant and extinction coefficient of the system.

These systems should be operated in an automatic way. With that idea in our mind, we have developed a software system which, once calibrated for each instrument, is able to analyze without user intervention all the images produced with such systems. Since the software is open source, everyone will be able to improve it or check its results in the future.

All-sky cameras can operate autonomously for longer periods of time, obtaining robust and statistically significant data about astronomical conditions on a given site. We have presented the results of the analysis for one of these sites, Teide Observatory. These results have been used in the spanish CTA group to defend in the CTA consortium the position of Izaña as a candidate to host CTA-North.

Some of the measures we have done include:

- Long term statistics on night sky background, extinction and cloud coverage in Johnson B, V and R bands.
- Comparison of extinction coefficients between a clear night and a night with Saharan dust.
- Comparison between IAC80 telescope and AstMon night sky background measures at Teide Observatory.
- Moonlight effect on the night sky background in different bands, its dependence with Moon position and phase and its possible uses in exposure calculators and Cherenkov astronomy.
- Milky way effect modelization in Johnson B, V and R bands.

We have also pointed some of the limitations of AstMon-OT. The quality of B band background data would increase with longer exposure times due to the increase in SNR and the lesser effect of image bias fluctuations of Figure 3.2. New flatfields should be generated to remove any doubt of uncorrected system vignetting. Finally, the long-term analysis should be repeated for the all-sky data with spatial resolution. This will let us to study properly effects like the solar activity influence on night sky background.

Acknowledgements

Part of the work has been performed using the facilities of Laboratorio de Investigación Científica Avanzada (LICA-UCM) of the Moncloa Campus of International Excellence (UCM-UPM).

We acknowledge the support and the access to the instrumentation provided by Instituto de Astrofísica de Canarias (IAC).

The project was partially funded by MICINN under project FPA2010-22056-C06-06.

Bibliography

- [1] Mait Lang et al. Canopy gap fraction estimation from digital hemispherical images using sky radiance models and a linear conversion method. *Agricultural and Forest Meteorology, Volume 150, Issue 1*, January 2010. URL <http://www.sciencedirect.com/science/article/pii/S0168192309001920>.
- [2] Michael S. Bessel. Standard photometric systems. *Astronomy and Astrophysics, 2005, 43*, 2009. URL http://www.astrohandbook.com/ch02/bessell_photosystems.pdf.
- [3] Astro-Caltech Webpage,. URL <http://www.astro.caltech.edu/palomar/lp.html>.
- [4] IAC Webpage,. URL <http://www.iac.es/servicios.php?op1=28&op2=69>.
- [5] IAC Webpage,. URL <http://www.iac.es/adjuntos/otpc/leycielo.pdf>.
- [6] IAC Webpage,. URL <http://www.iac.es/adjuntos/otpc/folletolc.pdf>.
- [7] Thomas Lepoutre Jean Clairambault, Stephane Gaubert. Representations of celestial coordinates in fits. *Mathematical and Computer Modelling, Volume 53, Issues 7-8*, pages 1558–1567, April 2011. URL <http://arxiv.org/abs/astro-ph/0207413>.
- [8] David E. Blask et al. Melatonin-depleted blood from premenopausal women exposed to light at night stimulates growth of human breast cancer xenografts in nude rats. *American Association for Cancer Research.*, September 2005. URL <http://cancerres.aacrjournals.org/content/65/23/11174.abstract>.
- [9] Brad Scriber. Light pollution. *National Geographic*, October 2008. URL http://ngm.nationalgeographic.com/geopia/Light_Pollution.
- [10] Lightscape / night sky. *National Park Service*. URL <http://www.nps.gov/grba/naturescience/lightscape.htm>.
- [11] Mark R. Calabretta and Eric W. Greisen. Representations of celestial coordinates in fits. *Astronomy & Astrophysics*, page 14, February 2008. URL <http://arxiv.org/abs/astro-ph/0207413>.
- [12] Pablo Ramirez Moreta. Brillo de fondo de cielo con astmon-ucm. *E-Prints Complutense*, April 2012. URL <http://eprints.ucm.es/15000/>.
- [13] Miguel Nievas. Fotometría absoluta y brillo de fondo de cielo con astmon-ucm. *E-Prints Complutense*, November 2012. URL <http://eprints.ucm.es/16974/>.
- [14] Georgia Institute of Technology. Lecture 2. the beer-bouguer-lambert law. concepts of extinction (scattering plus absorption) and emission. schwarzschild's equation. URL http://irina.eas.gatech.edu/EAS8803_Fall2009/Lec2.pdf.
- [15] K. A. Pickering. The ancient star catalog. *The International Journal of Scientific History*, page 13, September 2002. URL <http://www.dioi.org/vols/wc0.pdf>.

- [16] M. R. Kidger et al. The atmospheric extinction profile in the canary islands: I - the visible extinction. *The Observatory*, Vol. 123, p. 145-150, June 2003. URL http://adsabs.harvard.edu/cgi-bin/nph-bib_query?bibcode=2003Obs...123..145K&db_key=AST&high=3f7e08976315206.
- [17] M. R. Kidger et al. The atmospheric extinction profile in the canary islands: I - the visible extinction. *The Observatory*, Vol. 126, p. 166-176, June 2006. URL http://adsabs.harvard.edu/cgi-bin/nph-bib_query?bibcode=2006Obs...126..166K&db_key=AST&high=3f7e08976315206.
- [18] Miguel Nievas and Rafael Barrena. Night sky background at the canarian observatories. *Unpublished*, 2013.
- [19] J. Aceituno et al. An all-sky transmission monitor: Astmon. 2011 *PASP*, 123:1076 - 1086, 2011. URL <http://digital.csic.es/bitstream/10261/56669/1/astron.pdf>.
- [20] Song Yao et al. Moon night sky brightness simulation for xinglong station. *arXiv:1304.7107v1 [astro-ph.IM]*, 2013. URL <http://arxiv.org/abs/1304.7107v1>.
- [21] Daniel Britzger et al. Studies of the influence of moonlight on observations with the magic telescope. *arXiv:0907.0973v1 [astro-ph.IM]*, 2009. URL <http://arxiv.org/abs/0907.0973>.
- [22] Kevin Krisciunas and Bradley E. Schaefer. A model of the brightness of moonlight. *Astronomical Society of the Pacific, Publications (ISSN 0004-6280)*, vol. 103, September 1991. URL <http://articles.adsabs.harvard.edu//full/1991PASP..103.1033K/0001033.000.html>.
- [23] Ferdinando Patat. Observing during bright time: tips and tricks. *Messenger* 118, 11, 14, 2004. URL <http://www.eso.org/sci/publications/messenger/archive/no.118-dec04/messenger-no118-11-14.pdf>.
- [24] J. Albert et al. Very high energy gamma-ray observations during moonlight and twilight with the magic telescope. *Astroparticle Physics*, February 2007. URL <http://arxiv.org/abs/astro-ph/0702475>.
- [25] F. Hroch. Rawtran. 2007. URL <http://integral.physics.muni.cz/rawtran/>.
- [26] Jaime Zamorano et al. Iss nocturnal images as a scientific tool against light pollution. *LICA report*, April 2011. URL <http://eprints.ucm.es/12729/>.
- [27] M. Emre Aydin. URL <https://github.com/eaydin/cr2fits>.

Appendix A

AstMon-UCM

A.1 Madrid. A light polluted sky

Universidad Complutense de Madrid's observatory (hereafter UCM Observatory) is located at Ciudad Universitaria, in Madrid city. It is therefore an urban observatory heavily affected by light pollution from human activity.

AstMon-UCM was installed in 2010, and its main objective is the characterization and study of the long-term evolution of light pollution in our city. In [13] we set-up the first release of our code in this device. Since July 2012 it is working autonomously, doing a full calibration for each observation night and obtaining the night sky background and extinction coefficients for Johnson B, V and R bands. The results of this analysis are published in our FTP server ftp://147.96.21.177/PyASB_v1/.

With the new release in production for AstMon-OT data, we tried to perform a similar analysis on AstMon-UCM, but due to the dataset size (we have more than 100k images in B, V and R bands), we have not yet completed the first phase (calibration) of the instruments, so the results in this section should be taken with care.

A.2 Night Sky Background

In Figure A.1 we show the measured Night Sky Background at zenith for AstMon-UCM data. As we pointed before, the statistical coverage is not complete yet, so we are not yet ready to study long-term variations on the NSB parameter.

From Table A.1, we see that for each background photon that reach the ground at Teide Observatory, we see at a light polluted site like UCM Observatory 24 photons in B band and 27 photons in V and R bands. This translates into a $\sim 5 \times$ factor in photon noise, which is critical if one wants to study the brightness of low surface-brightness sources.

Figure A.2 corresponds to the mean observed time evolution of the Night Sky Background along the night for Johnson V band.

	B	V	R
AstMon-OT ($mag/arcsec^2$)	22.32 ± 0.48	21.18 ± 0.53	20.59 ± 0.50
AstMon-UCM ($mag/arcsec^2$)	18.88 ± 0.80	17.59 ± 0.51	17.03 ± 0.39
Ratio (photons)	~ 24	~ 27	~ 27

TABLE A.1: Comparison of measured night sky background between OT and UCM sites.

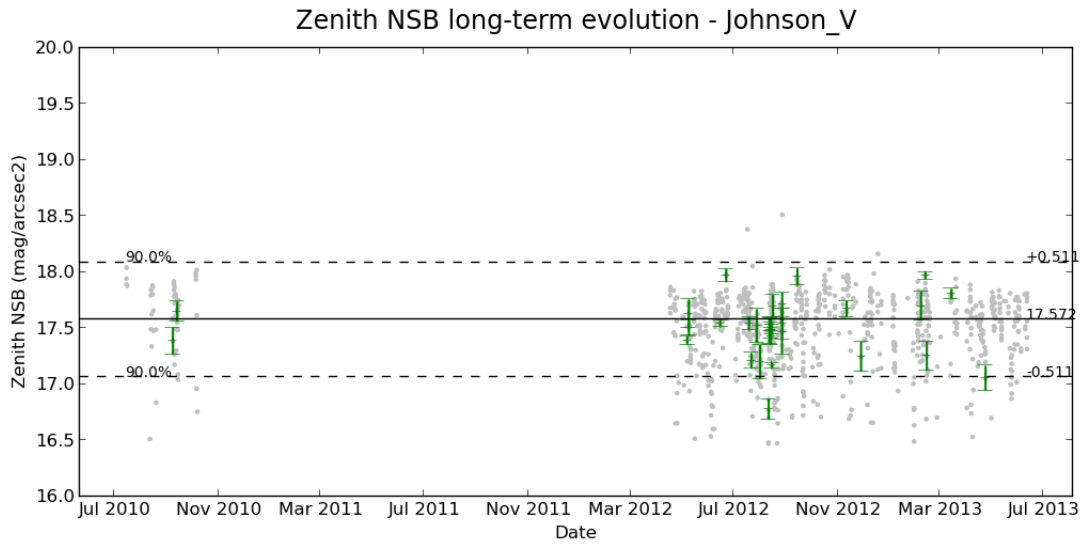


FIGURE A.1: Zenithal Night Sky Background evolution over the time from AstMon-UCM in V band. The median and the interval that contains the 90% of the data is given. Error bars are shown for some selected points as reference.

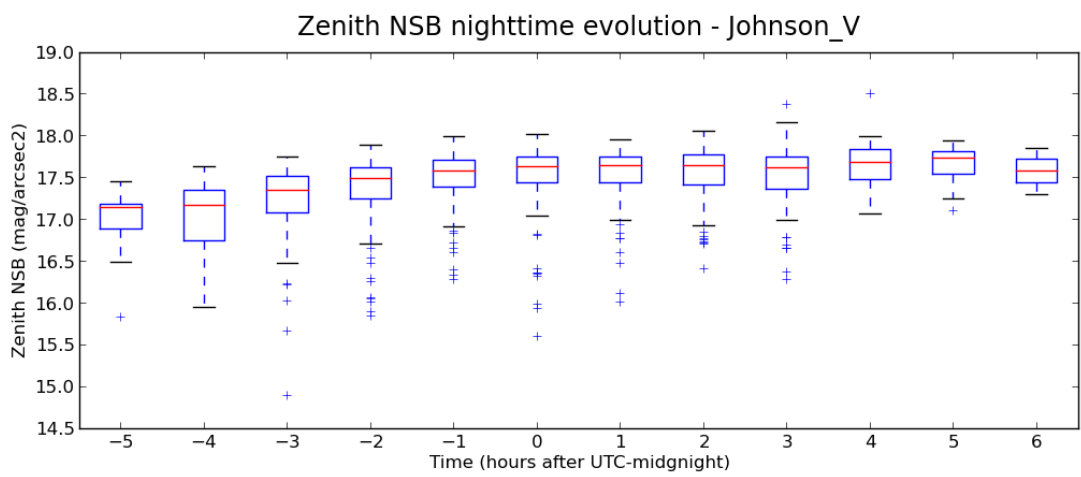


FIGURE A.2: Night sky background evolution over the night at UCM Observatory.

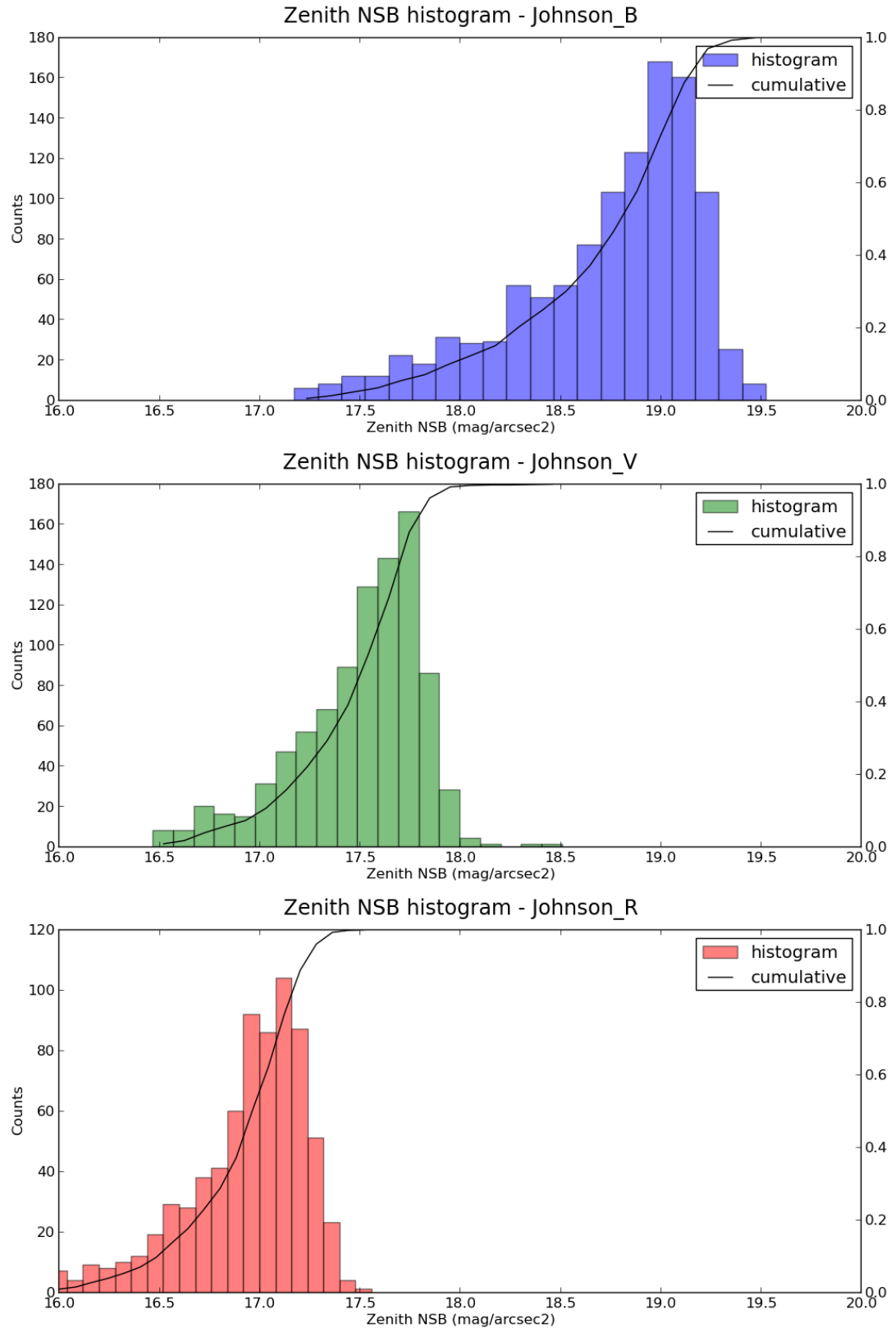


FIGURE A.3: Zenithal Night Sky Background histogram at UCM Observatory.

Appendix B

Digital Cameras on site testing

B.1 Description

Digital cameras (DSLR) are potential candidates for light pollution, night sky background and extinction monitors. They have all the ingredients we need for this task:

- Availability. Canon and Nikon models are actually very easy to acquire, ranging their cheapest bodies from ~ 300 euro. Nowadays, DSLR cameras are a product of consume and the vast majority of amateur astronomers have worked with them.
- Sensor size. From APS-C (bigger than the QSI 583WS used in AstMon) to Full-Frame ($35mm$ diagonal).
- They are able to produce long exposure images, can be operated directly by the user (portability) or with a computer (automatization).
- Built-in filters. The most common format is to have a R,G,B Bayer matrix in a RGGB layout. The response of filters depends on the camera model and manufacturer and will probably be different from the response of traditional photometric systems such as the Johnson-Cousins.

Monochrome CCDs on the other hand are expensive, they require complex computer programs to work and a good knowledge of their characteristics and use by the user. They require also a set of auxiliary devices like filter-wheels and a set of (at least) RGB filters.

The main advantage of the CCDs is the quality of the photometric data they provide. Their linearity is out of doubts, they are cooled (which reduces drastically the noise), they usually have more dynamic range (16 bits, DSLRs usually have 12-14bits) and they can be used with photometric filters.

The problem of the differences between RGB and Johnson systems can be solved with a proper calibration (with R,G,B photometric magnitudes for each star, calculated using their spectra) or with color correction terms. As a first approach, a linear correction is preferred,

$$\begin{bmatrix} B \\ V \\ R \end{bmatrix}_{synthetic} = \begin{bmatrix} \alpha_B^b & \alpha_B^g & \alpha_B^r \\ \alpha_V^b & \alpha_V^g & \alpha_V^r \\ \alpha_R^b & \alpha_R^g & \alpha_R^r \end{bmatrix} \times \begin{bmatrix} b \\ g \\ r \end{bmatrix}_{instrumental} \quad (B.1)$$

This calibration has been performed already by some researchers (see as an example the *rawtran* project[25]).

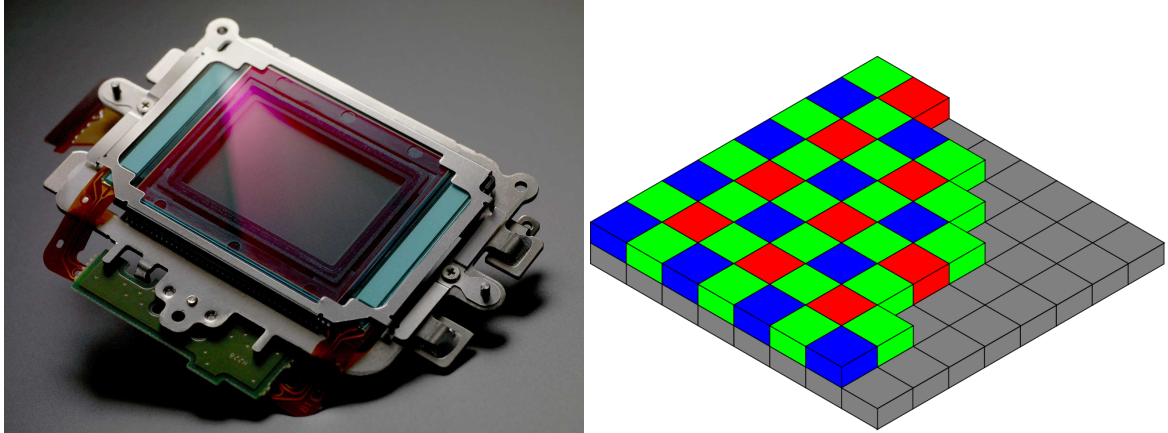


FIGURE B.1: **Left:** Digital camera sensor unit. IR-cut filter is visible (cyan color with purple reflection).
Right: Scheme of a Bayer matrix with RGGB layout in a sensor.



FIGURE B.2: **Left:** Set-up of a DSLR camera to obtain all-sky images. **Right:** Crop of Villaverde's night sky image with Canon EOS 5D II and Sigma 8mm fisheye.

As a first test, we will not bother about the blue and red filters, where the most differences with the Johnson system are expected, and we will just use the G channel, which some authors[26] have found to have a similar response to Johnson V's.

B.2 Testing PyASB with digital cameras

In this section, we report on the use of a Canon EOS 5D Mark II camera equipped with a Sigma 8mm fisheye lens. This lens has a very similar behavior and projection to the Sigma 4.5mm used in AstMon, but is optimized for large Full-Frame sensors.

```

-----
# Angle, illumination
000, 1.000
020, 0.91
040, 0.795
060, 0.66
080, 0.515
090, 0.410
100, 0.3
120, 0.2
180, 0.2
-----

```

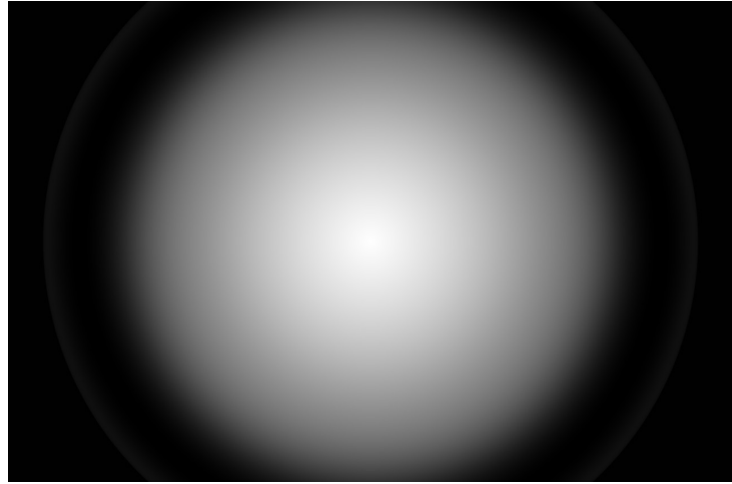


FIGURE B.3: **Left:** Vignetting table with the angle (from the optical axis) and the relative illumination. Values from $\text{Angle} > 90^\circ$ are invented, and their only purpose is to populate the non-illuminated parts of the image with valid float values. The real data ($< 90^\circ$) has been obtained from [1]. **Right:** Generated flat field for the Canon 5D camera with our software.

Like AstMon, digital cameras suffer from vignetting with certain lenses (the Sigma 8mm is not an exception) and dark current, which is critical since they usually operate at higher temperatures than AstMon.

In order to correct the vignetting, we have developed a python program capable to create synthetic flatfields from a set of zenithal angle - relative illumination measures, the astrometric solution for the system (needed to convert degrees to physical coordinates in the image sensor) and an example science frame (used to get the basic image properties such as the width and height)[B.3]. The dark current is estimated using the non-illuminated corners of the image.

B.3 Results

In this section, we present some of the results we have obtained with digital cameras. Since the use of these devices for night sky background characterization is rather experimental, we have not done yet any long-term survey with them. From Figure B.4, we get the following lessons:

1. It is possible to get night sky background measures and generate NSB maps with digital cameras using fisheye lenses.
2. PyASB software is not only useful with CCD data, but also with DSLR images. It can be used without doing any pre-processing in the image further to the channel extraction and interpolation from the Bayer matrix. We have built a simple script based on `cr2fits` from M. Emre Aydin[27]. Our version is able to extract R,G and B channels at the same time for both Canon and Nikon images and to populate the FITS header with the raw image meta-data.
3. G band can be assimilated as Johnson V. However, for R and B channels, color correction terms are necessary.
4. The photometric precision depends on the quality of the data fit. We have tested robust automatic estimators and least-square fit[Figure B.5] with the star fluxes from different images (all of them

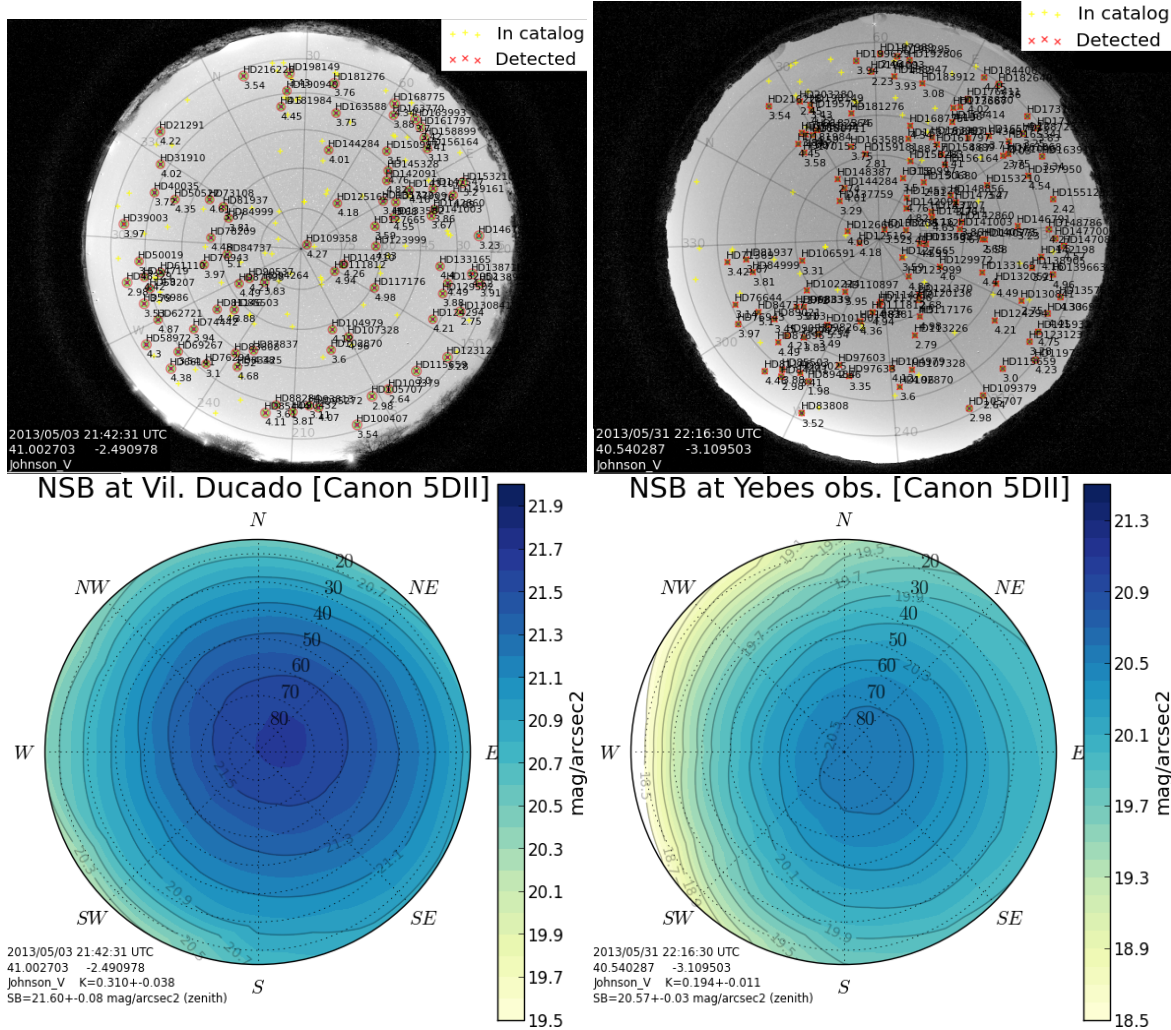


FIGURE B.4: Upper: Star detection process in Canon 5D Mark II + Sigma 8mm at Villaverde del Ducado (left) and Yebes astronomical center (right), both in Guadalajara but at different distances (100km and 50km) from Madrid. **Lower:** After calibrating the system with star fluxes, night sky background map is computed. Note the glow at West, caused by Madrid and Corredor del Henares light pollution. The glow is more prominent in Yebes (it is closer to Madrid).

with exposures in the range of 30s – 1m) manually filtered to remove outliers. In the ‘filtered’ LSQ fit[Figure B.5], we have found an intrinsic dispersion of the values of $m + 2.5 \log_{10} F$ for a single star of about 0.1^{mag} rms ($\sim 10\%$ of error in fluxes).

Figure B.5 shows the star photometric data measured with PyASB on images taken with a Canon EOS 5D Mark II digital camera working in SRAW1 format. The fisheye lens was a Sigma 8mm at f3.5 with exposures from 30 to 60s at ISO1600.

From [B.5], we see that for Yebes images $C \sim 12.15$ while for Villaverde’s $C \sim 12.28 \text{ mag/arcsec}^2$. This is not expected, because we have taken the images under the same instrumental conditions, but could be explained if we take into account the precision of the measures and some defects in the stars shapes due to anti-blooming in Villaverde’s image.

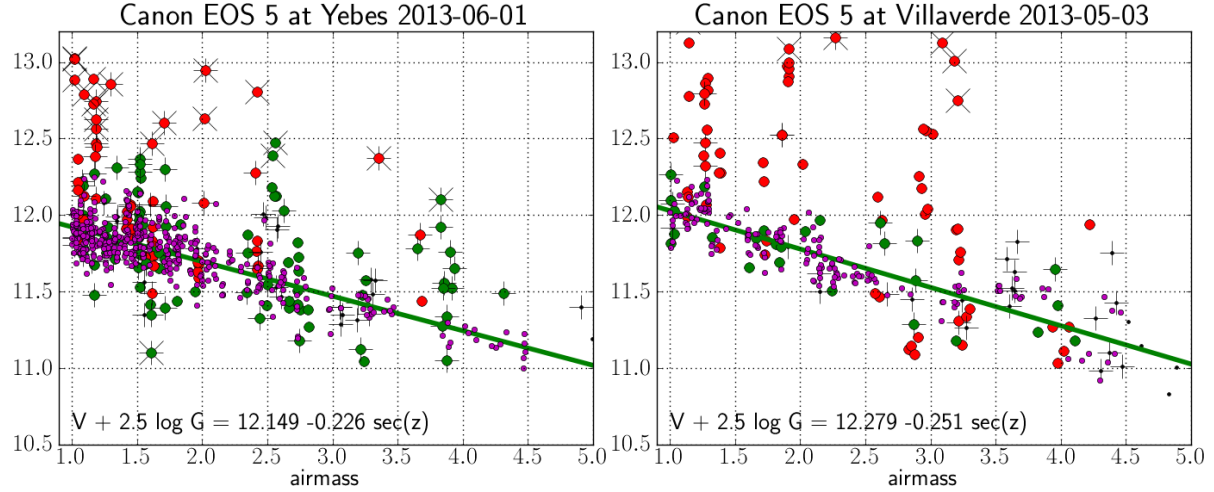


FIGURE B.5: Photometric fit of the data from two observations with the DSLR camera using similar parameters. The green linear fit is done for the filtered data (purple points) after removing variable stars (red points), low signal stars or those with less precision than 0.1^{mag} (crosses shaped points) and stars with more than 0.3^{mag} of differences between images. **Left:** Yebes astronomical center (Guadalajara, $\sim 50\text{km}$ from Madrid) data. **Right:** Villaverde del Ducado (Guadalajara, $\sim 130\text{km}$ from Madrid) data.

This calibration can be improved with a proper choice of exposure times or even better, doing multiple exposures, because it seems clear from the data that the star calibration process prefers fairly short exposures, but the background SNR increases with longer exposure times.

